JOURNAL OF PETROLOGY | VOLUME 43 | NUMBER 10 | PAGES 1923–1946 | 2002

Chemical Diversity of the Ueno Basalts, Central Japan: Identification of Mantle and Crustal Contributions to Arc Basalts

JUN-ICHI KIMURA[1]*, WILLIAM I. MANTON[2], CHIH-HSIEN SUN[2]†, SHIGERU IIZUMI[1], TAKEYOSHI YOSHIDA[3] AND ROBERT J. STERN[2]

[1]DEPARTMENT OF GEOSCIENCE, SHIMANE UNIVERSITY, MATSUE 690-8504, JAPAN

[2]GEOSCIENCES DEPARTMENT, UNIVERSITY OF TEXAS AT DALLAS, DALLAS, TX 75083-0688, USA

[3]INSTITUTE OF MINERALOGY, PETROLOGY AND ECONOMIC GEOLOGY, TOHOKU UNIVERSITY, AOBAKU, SENDAI 980-7763, JAPAN

RECEIVED JUNE 30, 2001; REVISED TYPESCRIPT ACCEPTED APRIL 11, 2002

The Ueno Basalts of central Japan comprise a monogenetic volcanic cone complex that was active between 2·76 and 1·34 Ma. Basalts were erupted at more than 14 centers scattered over a region 40 km in diameter. Alkali basalt was erupted first, followed by sub-alkaline basalt. Quasi-concentric expansion of eruption centers coinciding with uplift and with decreasing alkalinity of the lavas suggests that Ueno magmatism originated from a mantle diapir as it mushroomed at the base of the lithosphere. Depleted asthenospheric mantle (alkali basalt), enriched lithospheric mantle (sub-alkaline basalt), and crustal components are identified as chemical end-members in the petrogenesis of the Ueno Basalts. Incompatible trace element abundances indicate that the Ueno alkali basalts are typical within-plate basalts, whereas the sub-alkaline basalts show strong affinities with normal arc lavas. Sr–Nd–Pb isotopic compositions indicate that the mantle source of the alkali basalts was more depleted than that of the sub-alkaline basalts. About 7% melting of asthenospheric mantle in the garnet-lherzolite stability field produced the primitive alkali basalts and 12% melting of spinel lherzolite within the subcontinental lithosphere produced the primitive sub-alkaline basalts. Isotopic compositions and fluid mobile/immobile element ratios broadly covary with SiO_2 contents in the sub-alkaline suite, and increasing silica content is associated with stronger EMII (Enriched Mantle II) isotope affinities and fluid mobile element abundances. A progressive AFC (assimilation–fractional crystallization) model assuming assimilation of a low-K silicic melt reproduces the chemical variations observed in the sub-alkaline suite. Melting of a flattening mantle diapir at the base of the lithosphere is the dominant cause of Ueno magmatism, accompanied by the assimilation of older arc crust.

KEY WORDS: *arc basalt; crustal assimilation; mantle heterogeneity; Ueno Basalts*

INTRODUCTION

The Ueno Basalts erupted from a complex of monogenetic volcanoes in central Japan, and consist of alkali to sub-alkaline lavas thought to have originated from melting of a rising and flattening mantle diapir (Kimura & Yoshida, 1999). Volcanism began at 2·7 Ma and continued until 1·3 Ma (Ujike *et al.*, 1992; Kimura & Yoshida, 1999; Nakano *et al.*, 2000). Petrological and geochemical studies indicate that there are two distinct alkali and sub-alkaline magma types, with different mantle sources. The former are similar to within-plate basalts and the latter to typical island-arc basalts (Kimura & Yoshida, 1999; Nakano *et al.*, 2000; Ujike & Stix, 2000). Fractional crystallization alone cannot explain the chemical diversity of the sub-alkaline lavas, and the involvement of multiple crustal contaminants has been proposed (Nakano, 1993, 1994; Kimura & Yoshida, 1999; Nakano *et al.*, 2000; Ujike & Stix, 2000). The compositional diversity and well-understood tectonic setting and volcanology make this volcanic field appropriate for studying the origin of arc basalts. Here, we present new trace element and radiogenic isotope data for the Ueno Basalts and discuss the mantle and crustal processes that could account for the chemical diversity of the suite.

*Corresponding author. Telephone: +81 852 32 6462. Fax: +81 852 32 6462. E-mail: jkimura@riko.shimane-u.ac.jp

†Present address: Exploration and Development Research Institute, Chinese Petroleum Corporation, PO Box 166, Miaoli, Taiwan 360.

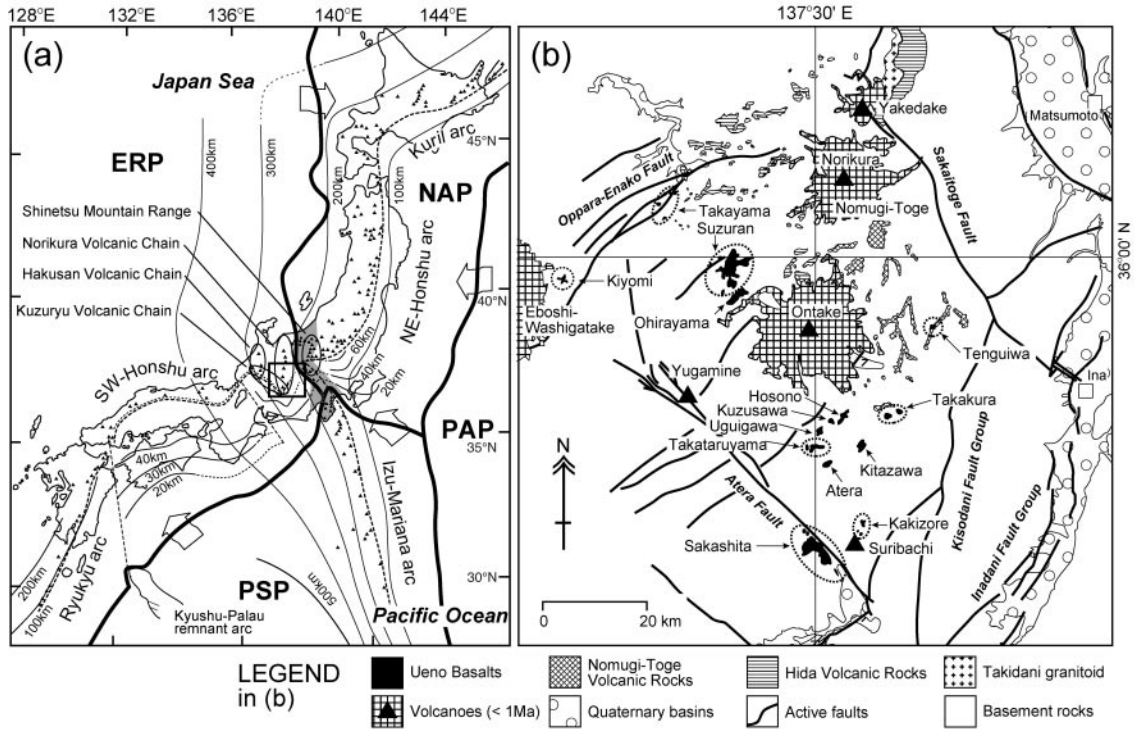

Fig. 1. Maps showing (a) the tectonic setting of Japan and the location of the Ueno Basalt province, and (b) the geology of the Ueno Basalt province. In (a): NAP, North America plate; PAP, Pacific plate; ERP, Eurasia plate; PSP, Philippine Sea plate; bold continuous line, plate boundary; fine continuous line with number (km), depth of subducting slab surface; dashed line, volcanic front; oval, volcanic chains and range; ▲, Quaternary volcano; shaded area, Fossa Magna. Square shows the location of (b). The legend pertains to (b). Ueno Basalts rest on Nohi Rhyolite, except for the Kiyomi center, which lies on the Mino Zone sedimentary rocks. All of the basalt bodies are monogenetic scoria falls and lava flows, or dikes and vent breccias. Centers are on or confined within four active faults, the Atera, Oppara–Enako, and Sakaitoge Faults, and the Kisodani Fault Group.

GEOLOGY OF THE UENO BASALTS

The Ueno Basalts occur at the south end of the Norikura Volcanic Chain in central Japan (Fig. 1). This part of Japan lies along the eastern edge of the Eurasia plate, which overlies the subducted Philippine Sea and Pacific plates (Aramaki & Ui, 1982; Kimura & Yoshida, 1999). The upper surface of the Philippine Sea plate is about 60 km and the Pacific plate is about 250 km below the Norikura Volcanic Chain (Fig. 1a). The Moho beneath the area lies at a depth of 35 km, so the crust is somewhat thicker than elsewhere in Japan, where it is about 30 km thick (Zhao *et al.*, 1992). The basement in this region mainly consists of Cretaceous to Paleogene Nohi Rhyolites and related plutons, metamorphic rocks of the Hida Belt, and the Mino Zone accretionary prism complex (Yamada, 1977; Hiroi, 1981; Otsuka, 1988; Yamada & Kobayashi, 1988; Harayama, 1990; Harayama *et al.*, 1991).

The Ueno basalt province lies in the Hida Mountains, an uplift on the western flank of the Fossa Magna (Fig. 1). Development of the Fossa Magna began about 15 Ma and was caused by bending of Honshu as the Japan Sea opened (Otofuji *et al.*, 1985, 1994). Eastward drift of Japan was also associated with collision of the Izu arc with central Honshu, causing uplift in the middle part of the Fossa Magna (Matsuda, 1978). Regional uplift of the entire Fossa Magna began at ~8 Ma. Differential uplift of the Hida Mountains began at ~3·8 Ma with formation of a major boundary fault, the Itoigawa–Shizuoka Tectonic Line, which is also the Eurasia–North America plate boundary (Fig. 1) (Takeuchi, 1995).

Volcanic activity in the Hida Mountains began at ~5 Ma (Shimizu & Itaya, 1993). Pliocene activity was concentrated in the Kuzuryu Volcanic Chain to the west of the Hida Mountains (Fig. 1a). Activity migrated to the main uplift axis of the Hida Mountains (the Norikura Volcanic Chain) at ~2·8 Ma when the Ueno Basalts were erupted together with the Nomugi–Toge Volcanic Rocks (andesite to rhyolite), and the Hida Volcanic Rocks (dacite to rhyolite) (Shimizu & Itaya, 1993; Kimura & Yoshida, 1999; Kimura *et al.*, 1999). Activity in the Norikura Volcanic Chain continued until ~1·3 Ma (Shimizu & Itaya, 1993; Nakano *et al.*, 2000). After

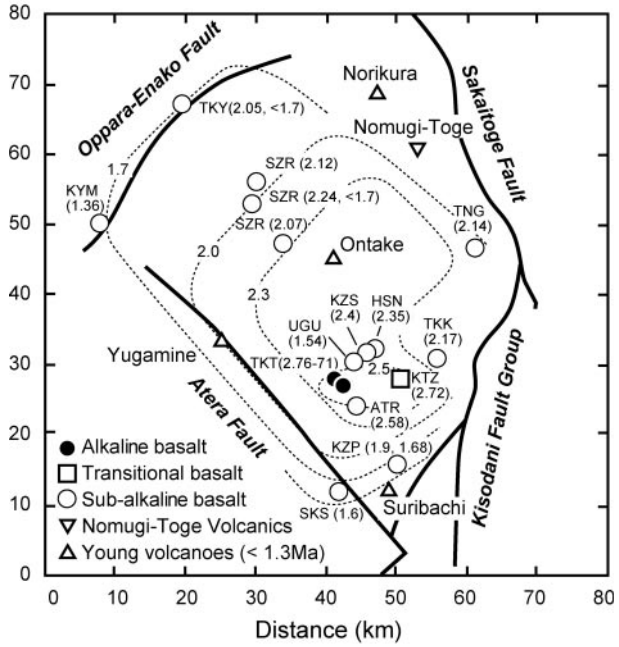

Fig. 2. Distribution of eruption ages (in parentheses, in millions of years BP; data sources: Ujike *et al.*, 1992; Shimizu & Itaya, 1993; Nakano *et al.*, 2000) for the Ueno Basalts. Eruptions started with alkali and transitional basalt south of Ontake and activity migrated outwards and changed to sub-alkaline compositions with time. Regional uplift in the central part coincided with this activity (Kimura & Yoshida, 1999). KYM, Kitomi; TKY, Takayama; SZR, Suzuran; TNG, Tengu; HSN, Hosono; KZS, Kuzusawa; UGU, Ugui; TKK, Takakurayama; TKT, Takataruyama; KTZ, Kitazawa; ATR, Atera; KZP, Kakuzore Pass; SKS, Sakashita. Dotted line with numbers: age contours showing spread of the eruption centers with time.

~1 Ma, stratovolcanoes with intermediate compositions began to grow in the Norikura Volcanic Chain, including five stratovolcanoes with four cones.

The Ueno Basalt province is distributed around Ontake, a large Quaternary stratovolcano in the southern Norikura Volcanic Chain. The Quaternary volcanoes of this chain are Norikura (<1·3 Ma; Nakano *et al.*, 2000), Ontake (<0·75 Ma; Matsumoto & Kobayashi, 1999), and a basalt stock at Suribachi (0·9 Ma; Ujike *et al.*, 1992), all of which are younger than the Ueno Basalts (Fig. 1b). Nakano (1993, 1994) and Kimura & Yoshida (1999) studied Ueno Basalt geology, and identified 14 eruption centers: Sakashita, Kakizore, Atera, Kitazawa, Takataruyama, Uguigawa, Kuzusawa, Hosono, Takakura, Tenguiwa [termed Kamiogawa by Nakano *et al.* (2000)], Ohirayama, Suzuran, Kiyomi [Naradani of Nakano *et al.* (2000)], and Takayama (Fig. 1b). Each center is composed of a small volume (<3 km^3) of basalt to basaltic andesite lava flows, scoria fall deposits, and dikes (Nakano, 1993, 1994; Kimura & Yoshida, 1999). The eruption centers are scattered over a 40 km radius approximately centered on Ontake volcano, and are restricted to a hexagonal basement block bounded by four major active faults: the Atera, Oppara–Enako, Sakaitoge Faults, and Kisodani Fault Group (Fig. 1b).

The Ueno Basalts range in age from 2·76 to 1·36 Ma (dated by K–Ar; Ujike *et al.*, 1992; Shimizu & Itaya, 1993; Kimura & Yoshida, 1999; Nakano *et al.*, 2000). The K–Ar ages agree with magnetostratigraphy and tephrochronological relationships (Kimura & Yoshida, 1999). Periodic eruptions continued for over 1·5 Myr (Ujike *et al.*, 1992; Shimizu & Itaya, 1993; Kimura & Yoshida, 1999; Nakano *et al.*, 2000). The first eruptions occurred in the southeastern portion of the province (Ujike *et al.*, 1992), and activity migrated outwards quasi-concentrically with time (Kimura & Yoshida, 1999; Nakano *et al.*, 2000) (Fig. 2). Uplift coincided with the migration of volcanism, suggesting that volcanism and uplift began when a mantle diapir reached the base of the lithosphere and spread out as it flattened (Kimura & Yoshida, 1999).

PETROGRAPHY OF THE UENO BASALTS

The Ueno Basalts are classified petrographically as olivine basalt, olivine–clinopyroxene (cpx) basalt, and plagioclase–olivine–cpx basaltic andesite. Olivine basalts sometimes contain skeletal olivine. Olivine crystals contain chromian spinel inclusions, and clinopyroxene occasionally has sector zoning. Basalt from the Takataruyama center contains hornblende pseudomorphs, most of which show subrounded but resolved shapes. Pseudomorph interiors consist of tiny plagioclase, pyroxene, magnetite, and olivine crystals with trace amounts of glass. Plagioclase phenocrysts occur in basaltic andesites, along with olivine and cpx. Plagioclase laths and magnetite are the groundmass minerals. Basaltic andesites also commonly contain magnetite and ilmenite phenocrysts. Ueno basalts contain 5–10 vol. % phenocrysts, consisting of 3–10% olivine, 0–4% cpx, and 0–0·4% plagioclase (Nakano, 1993, 1994; Kimura & Yoshida, 1999; Nakano *et al.*, 2000; Ujike & Stix, 2000).

Olivine compositions vary from $Fo_{90–80}$ in cores to $Fo_{65–70}$ in rims. Clinopyroxene is normally zoned, with Mg-numbers ranging from 75 to 80. Plagioclase compositions range from An_{72} to An_{87}, and almost all are normally zoned. Basaltic andesites typically contain Mg-poor phases. These are $Fo_{65–75}$ in olivine, Mg-number 70–80 in cpx, and $An_{65–77}$ in plagioclase (Nakano, 1993, 1994; Kimura & Yoshida, 1999; Nakano *et al.*, 2000; Ujike & Stix, 2000).

COMPOSITION OF THE UENO BASALTS

Kimura & Yoshida (1999) reported major element compositions of 113 samples of Ueno Basalts. We analyzed trace elements (Ba, Ce, Co, Cr, Ga, Nb, Ni, Pb, Rb, Sr, Th, V, Y, Zr) of the same 113 samples using X-ray fluorescence spectrometry (Rigaku, RIX2000 at Fukushima University) following the method described by Kimura & Yamada (1996). Selected samples were analyzed for additional trace elements [Li, Be, Rb, Y, Zr, Nb, Mo, Sn, Sb, Cs, rare earth elements (REE), Hf, Ta, Tl, Pb, Th, U] and Sr, Nd, and Pb isotope compositions. Trace elements were analyzed using inductively coupled plasma mass spectrometry (Thermo ELEMENTAL, VG PQ3 at Shimane University) by the standard addition technique and using the normal concentric nebulizer (Kimura *et al.*, 1995). The acid digestion process was partly modified from Kimura *et al.* (1995), using 1:1 $HClO_4$ and HF for digestion and mixed acids (HNO_3, HCl, with trace HF) for better element recovery (Münker, 1998). Sr and Nd isotope ratios were determined by thermal ionization mass spectrometry (TIMS) (Thermo Quest Finnigan MAT 262 at Shimane University) following methods described by Iizumi *et al.* (1994, 1995). Pb isotope ratios were also measured by TIMS (Finnigan MAT 261 at the University of Texas at Dallas) following the methods of Manton (1988). Isotope ratios of standards determined during the analysis of the samples were: NIST SRM987 Sr: $^{87}Sr/^{86}Sr = 0{\cdot}710221 \pm 61$ (2σ; $n = 7$); La Jolla Nd: $^{143}Nd/^{144}Nd = 0{\cdot}511867 \pm 34$ (2σ; $n = 5$), NIST SRM981 Pb: $^{206}Pb/^{204}Pb = 16{\cdot}928 \pm 14$, $^{207}Pb/^{204}Pb = 15{\cdot}481 \pm 16$, $^{208}Pb/^{204}Pb = 36{\cdot}658 \pm 41$ (2σ; $n = 3$). Analytical results are shown in Table 1.

Major element compositions

Nakano (1993, 1994) and Kimura & Yoshida (1999) reported major element compositions for the Ueno Basalts. The SiO_2 contents range from 47 to 54 wt %. All the Ueno Basalts are classified as basalt or basaltic andesite using TAS (total alkali–silica) criteria (Le Maitre *et al.*, 1989). Further classification of the basalts was also made based on alkali contents and normative compositions. The most alkali-rich Takataruyama basalt is nepheline-normative (TKT2B; Table 2). This sample is from a basalt dike. Three other samples from the same dike (TKT and TKT2 series) are also classified into the 'alkaline basalt' suite because of chemical similarity. Most Ueno lavas are olivine tholeiite (i.e. olivine-normative; sub-alkaline basalt; Miyashiro, 1978) (Fig. 3; Table 2). These lavas are classified as 'sub-alkaline basalts'. Five of six samples from Kitazawa and samples from Takataruyama (TKTA series) are transitional between the two suites and classified as 'transitional basalts'. These lavas fall in the alkali basalt field in a total alkalis vs SiO_2 plot (Fig. 3f). They are olivine normative but poor in normative hypersthene (i.e. TKTB; Table 2). Basaltic andesites from the Kiyomi, Ugui, and Atera centers are exceptionably quartz-normative (KYM5B, UGU1B, and ATR1A; Table 2). The occurrence of quartz-normative lavas is mostly limited to the outer perimeter of the Ueno Basalt province.

Incompatible major oxides, such as K_2O and Na_2O, are relatively constant in the sub-alkaline basalt suite (Nakano, 1994; Kimura & Yoshida, 1999), except for a relatively higher K group from the Sakashita and Kiyomi centers at the perimeter of the province (Fig. 3e). Even so, all the basalts are medium-K (Gill, 1981). Mg-numbers [= Mg/(Mg + Fe) molar ratio] range from 0·50 to 0·55 for alkali basalts and from 0·55 to 0·63 for sub-alkaline basalts (SiO_2 <52 wt %), suggesting modest fractionation of mafic minerals (Table 2). Some Ueno basalt compositions could have been in equilibrium with upper-mantle peridotite (Nakano, 1994; Kimura & Yoshida, 1999). Sub-alkaline basalt from Kitazawa has >10% MgO, high Ni and Cr contents, and contains Fo_{90} olivine, and so is thought to be primitive (Table 1). Other basaltic andesites (SiO_2 >52 wt %) are low in Mg-number (0·38–0·52), Ni, Cr and Fo in olivine, suggesting that these are differentiated or contaminated (Nakano, 1994; Kimura & Yoshida, 1999). Major high field strength elements (HFSE), such as Ti and P, have higher concentrations in alkali basalt than in sub-alkaline basalt.

Trace elements

Trace element compositions of the alkali basalts show convex-upward patterns when plotted on a primitive mantle-normalized trace element variation diagram [values from Sun & McDonough (1989)] (Fig. 4). Negative anomalies exist for Rb, U, K, and Sr. Sub-alkaline basalts have curvilinear patterns that are enriched in large ion lithopile elements (LILE), with negative Nb and Ta anomalies and positive Pb and Sb spikes. Except for anomalies in some LILE, the alkali basalts are compositionally close to within-plate basalts (WPB), whereas the sub-alkaline basalts possess typical island-arc basalt (IAB) signatures.

LILE ratios K/Rb, K/Ba, Ba/La, and Sr/Nd may reflect either magma source ratios or contamination of basalt magmas on the way to the surface. The values are K/Rb = 497–892 (average 581), K/Ba = 14·7–34·7 (25·3), Ba/La = 6·0–9·1 (8·1), Sr/Nd = 12·5–16·7 (23·9) for alkali basalts; K/Rb = 257–1679 (499), K/Ba = 20·6–50·8 (36·9), Ba/La = 8·2–33 (13·0), Sr/Nd = 17·9–33 (23·9) for sub-alkaline basalts (Table 1). Average LILE ratios are higher for sub-alkaline basalts

Table 1: Major and trace element and isotopic compositions of the Ueno Basalt lavas

Sample:	TKTA	TKTC	TKT2A	SKS1D	SKS6A	SKS7A	KYM5B	KYM5C	TKY1D
Age (Ma):	2·75	2·75	2·75	1·6	1·6	1·6	1·4	1·4	2·05
XRF wt %									
SiO_2	46·17	49·47	46·05	53·86	51·84	50·22	52·01	54·65	51·71
TiO_2	2·04	1·73	2·36	1·35	1·22	1·28	1·27	0·97	1·14
Al_2O_3	19·74	16·53	14·93	17·30	16·23	16·08	17·78	18·36	16·38
Fe_2O_3	13·00	11·78	14·08	9·59	10·65	10·40	11·51	9·30	10·23
MnO	0·23	0·19	0·21	0·17	0·17	0·17	0·24	0·16	0·16
MgO	8·07	7·26	7·03	4·01	6·56	8·97	3·86	3·22	7·62
CaO	7·31	8·53	9·25	7·90	8·65	8·81	9·34	7·45	8·95
Na_2O	2·30	3·11	3·27	3·31	3·01	3·02	3·01	3·69	2·87
K_2O	0·52	0·93	0·76	1·43	0·97	0·57	1·31	0·97	0·73
P_2O_5	0·82	0·70	1·14	0·30	0·37	0·29	0·34	0·63	0·31
Total	100·75	100·23	99·07	99·23	99·66	99·81	100·65	99·40	100·09
XRF (ppm)									
Ba	293	222	239	376	228	127	264	374	160
Ce	75	58	89	32	31	29	35	64	28
Co	50	42	42	28	41	44	34	24	39
Cr	310	266	145	19	231	487	47	25	339
Ga	24	21	23	20	19	16	19	20	18
Nb	22	19	37	6	8	5	6	12	6
Ni	94	86	70	7	82	187	18	16	112
Pb	4	5	3	6	4	3	5	7	3
Rb	4	21	14	36	22	7	30	21	17
Sr	582	566	691	561	466	475	632	855	414
Th	3	3	5	4	1	1	4	2	2
V	270	244	244	256	185	220	254	87	210
Y	47	32	37	26	24	31	23	17	27
Zr	270	234	377	139	167	133	134	290	130
ICP-MS (ppm)									
Li	9·60	8·09	8·77	9·73	8·02	7·07	5·80	6·77	—
Be	1·28	1·40	1·95	1·08	1·08	0·89	1·02	1·36	—
Rb	4·80	21·8	12·7	35·2	23·6	6·8	28·0	20·0	—
Y	36·7	27·5	31·3	21·3	23·2	23·5	18·8	16·1	—
Zr	270	272	393	122	152	116	118	238	—
Nb	21·2	18·9	26·9	6·0	7·3	4·9	5·4	12·6	—
Mo	—	1·04	1·47	1·00	—	0·83	1·24	1·83	—
Sn	1·70	1·48	2·63	1·21	1·42	0·94	1·36	0·89	—
Sb	0·05	0·17	0·29	0·14	0·34	0·18	0·31	0·23	—
Cs	0·25	0·60	0·32	1·14	0·96	0·22	1·20	0·41	—
La	32·1	24·5	39·6	15·6	18·8	13·3	14·4	28·6	—
Ce	70·7	64·2	108	34·0	40·8	25·9	33·5	67·3	—
Pr	10·0	7·96	13·4	4·53	5·49	3·94	4·33	7·76	—
Nd	41·7	34·0	55·1	19·5	22·4	18·0	19·2	31·1	—
Sm	8·63	6·93	10·4	4·25	4·86	4·05	4·28	4·90	—
Eu	2·68	2·29	3·31	1·55	1·62	1·52	1·44	1·90	—
Gd	8·22	7·10	10·4	4·47	5·04	4·13	4·22	5·79	—
Tb	1·20	1·14	1·56	0·81	0·71	0·79	0·73	0·75	—
Dy	6·64	6·52	8·08	4·74	4·15	4·65	4·28	4·16	—
Ho	1·28	1·00	1·17	0·85	0·84	0·84	0·74	0·62	—
Er	3·64	2·93	3·32	2·39	2·45	2·40	2·09	1·90	—
Tm	0·48	0·38	0·41	0·34	0·34	0·33	0·29	0·25	—
Yb	3·04	2·48	2·60	2·33	2·17	2·13	1·92	1·72	—
Lu	0·44	0·36	0·37	0·35	0·32	0·33	0·29	0·27	—
Hf	6·00	5·32	8·67	3·36	3·64	2·96	3·11	5·79	—
Ta	1·22	1·11	2·17	0·42	0·44	0·31	0·34	0·75	—
Tl	0·03	0·08	0·07	0·09	0·13	0·04	0·27	0·05	—
Pb	5·58	4·88	4·75	7·33	5·13	5·61	6·40	6·98	—
Th	2·64	2·33	1·56	3·85	2·17	1·18	2·72	3·09	—
U	0·33	0·58	0·41	0·72	0·51	0·30	0·60	0·70	—
TIMS isotope ratios									
$^{87}Sr/^{86}Sr$	0·70553	0·70550	0·70510	0·70607	0·70652	0·70490	0·70592	0·70756	0·70700
$^{143}Nd/^{144}Nd$	0·51284	0·51285	0·51290	0·51264	0·51282	0·51282	0·51265	0·51251	0·51267
εNd	—	4·16	5·14	0·05	—	3·56	0·24	−2·48	—
$^{206}Pb/^{204}Pb$	—	18·381	18·382	18·408	—	18·331	18·423	18·413	—
$^{207}Pb/^{204}Pb$	—	15·595	15·572	15·613	—	15·578	15·615	15·601	—
$^{208}Pb/^{204}Pb$	—	38·591	38·503	38·749	—	38·638	38·745	38·658	—

Table 1: continued

Sample:	TKY1E	TKTC	TKKB	TNG	HSNA	HSNE	KZP5C	KZP6B	KTZA
Age (Ma):	2·05	2·17	2·17	2·3	2·35	2·35	1·9	1·9	2·72
XRF wt %									
SiO_2	51·58	49·42	49·57	49·08	51·12	51·75	50·32	51·04	48·30
TiO_2	1·15	1·24	1·21	1·61	1·49	1·41	1·40	1·39	1·38
Al_2O_3	16·79	15·10	15·64	17·47	15·92	16·50	16·87	17·24	14·99
Fe_2O_3	10·45	11·12	11·56	10·32	10·85	10·02	10·44	10·23	11·17
MnO	0·16	0·18	0·16	0·17	0·17	0·17	0·17	0·16	0·18
MgO	7·45	9·53	8·62	7·61	7·21	6·47	7·25	6·92	9·44
CaO	8·46	9·22	8·66	9·18	8·29	8·42	8·98	8·39	9·46
Na_2O	2·74	2·82	2·91	3·16	3·29	3·51	3·29	3·31	2·78
K_2O	0·75	0·76	0·70	0·59	0·86	0·82	0·71	0·78	0·97
P_2O_5	0·31	0·32	0·37	0·50	0·49	0·45	0·35	0·38	0·37
Total	99·84	99·72	99·40	99·67	99·68	99·52	99·77	99·82	99·03
XRF (ppm)									
Ba	198	133	138	236	213	187	120	129	214
Ce	27	28	27	43	39	38	27	29	39
Co	39	46	44	41	44	38	43	42	45
Cr	354	599	490	255	292	214	260	257	382
Ga	18	16	18	22	20	18	17	18	15
Nb	7	6	7	12	12	9	6	6	11
Ni	117	184	174	110	119	98	97	98	118
Pb	4	4	1	6	3	5	3	3	5
Rb	17	24	21	3	18	15	13	16	31
Sr	398	422	467	625	575	626	414	416	447
Th	3	3	2	1	0	4	1	0	9
V	219	233	231	199	181	168	187	174	257
Y	29	30	24	24	29	23	26	27	21
Zr	130	119	127	185	190	181	145	160	129
ICP-MS (ppm)									
Li	4·57	6·50	7·88	5·73	7·80	8·18	6·84	—	8·35
Be	0·83	0·74	0·84	0·91	1·21	1·18	0·95	—	1·00
Rb	15·2	21·8	22·7	2·9	18·0	18·2	13·2	—	28·1
Y	21·8	24·2	19·9	21·4	28·2	23·3	25·6	—	19·2
Zr	112	106	124	171	167	168	137	—	133
Nb	5·6	6·6	7·0	11·4	11·3	9·8	5·5	—	12·0
Mo	0·80	0·99	1·03	0·63	1·19	1·00	0·89	—	1·42
Sn	1·02	1·09	0·91	1·17	1·35	1·22	1·16	—	1·35
Sb	0·21	0·23	—	0·06	0·19	—	0·12	—	0·28
Cs	0·75	0·84	0·83	0·19	0·49	0·47	0·22	—	1·21
La	12·5	16·3	12·9	18·7	23·6	16·9	10·3	—	15·4
Ce	26·3	28·8	31·1	44·8	44·9	41·1	25·5	—	36·7
Pr	4·38	4·81	4·63	6·36	7·46	6·06	3·80	—	4·82
Nd	19·3	21·1	20·7	25·8	32·2	26·6	18·1	—	21·2
Sm	4·47	4·76	4·91	5·89	6·84	6·13	4·39	—	4·55
Eu	1·61	1·67	1·60	1·93	2·43	2·10	1·57	—	1·55
Gd	4·39	4·88	4·63	5·82	6·92	5·57	4·37	—	4·54
Tb	0·80	0·85	0·66	0·95	1·14	0·78	0·88	—	0·78
Dy	4·80	4·95	4·15	5·18	6·28	4·73	5·23	—	4·38
Ho	0·84	0·86	0·76	0·83	1·03	0·90	0·95	—	0·72
Er	2·36	2·36	2·10	2·31	2·85	2·44	2·73	—	2·10
Tm	0·33	0·33	0·31	0·31	0·37	0·34	0·39	—	0·28
Yb	2·17	2·17	1·84	2·06	2·41	2·14	2·62	—	1·86
Lu	0·32	0·31	0·27	0·31	0·35	0·30	0·38	—	0·28
Hf	2·96	2·88	3·01	4·07	4·26	3·93	3·24	—	3·19
Ta	0·35	0·41	0·39	0·76	0·70	0·55	0·36	—	0·78
Tl	0·09	0·06	—	0·02	0·06	—	0·04	—	0·11
Pb	4·79	5·26	1·26	6·13	6·44	4·49	7·12	—	6·50
Th	1·58	1·84	1·81	2·51	2·06	1·71	1·14	—	2·40
U	0·39	0·47	0·50	0·30	0·54	0·52	0·33	—	0·70
TIMS isotope ratios									
$^{87}Sr/^{86}Sr$	0·70700	0·70557	0·70577	0·70609	0·70596	0·70600	0·70552	0·70564	0·70442
$^{143}Nd/^{144}Nd$	0·51267	0·51281	0·51280	0·51282	0·51280	0·51280	0·51283	0·51282	0·51289
εNd	0·64	3·37	—	3·57	3·18	—	3·75	—	4·94
$^{206}Pb/^{204}Pb$	18·429	18·364	—	18·366	18·357	—	18·315	—	18·314
$^{207}Pb/^{204}Pb$	15·649	15·576	—	15·573	15·580	—	15·566	—	15·560
$^{208}Pb/^{204}Pb$	38·841	38·522	—	38·504	38·534	—	38·428	—	38·394

Sample:	KTZF	SZR8B	ATR2B	ATR2F	UGU1A	UGU2B	KZS1C	KZS1D
Age (Ma):	2·72	2·15	2·53	2·53	1·6	1·6	2·3	2·3
XRF wt %								
SiO_2	47·19	51·23	52·72	50·41	52·36	54·17	54·24	54·17
TiO_2	1·51	1·31	1·22	1·38	1·23	1·12	1·41	1·38
Al_2O_3	15·01	17·00	16·99	16·90	17·30	17·48	18·40	18·09
Fe_2O_3	12·54	10·39	9·46	10·31	9·76	9·35	9·31	9·64
MnO	0·18	0·18	0·15	0·17	0·17	0·17	0·18	0·17
MgO	8·93	7·33	6·03	7·69	5·49	4·69	3·04	3·02
CaO	10·06	8·83	8·57	8·75	8·62	7·68	7·75	7·88
Na_2O	2·79	2·85	3·30	2·97	3·54	3·55	3·63	3·67
K_2O	0·71	0·60	0·87	0·72	0·79	0·88	1·43	1·45
P_2O_5	0·37	0·31	0·44	0·43	0·46	0·43	0·38	0·37
Total	99·29	100·03	99·74	99·73	99·72	99·51	99·76	99·84
XRF (ppm)								
Ba	158	134	142	151	190	247	360	358
Ce	31	25	32	35	36	45	30	36
Co	46	40	36	45	35	34	29	24
Cr	462	279	220	311	118	98	15	13
Ga	17	18	20	19	22	22	21	21
Nb	8	6	9	9	9	10	7	7
Ni	123	96	76	109	48	51	10	8
Pb	3	5	3	4	5	6	5	7
Rb	13	6	19	8	19	22	35	34
Sr	510	419	509	473	596	604	619	613
Th	2	2	0	1	1	1	2	2
V	270	214	159	202	167	154	171	174
Y	25	31	21	23	23	23	23	23
Zr	115	139	165	166	182	198	170	170
ICP-MS (ppm)								
Li	5·72	6·07	5·64	—	7·90	—	—	9·73
Be	0·80	0·86	0·99	—	1·09	—	—	1·28
Rb	13·9	4·2	18·5	—	19·7	—	—	38·9
Y	19·1	24·7	20·2	—	23·0	—	—	24·2
Zr	103	126	145	—	166	—	—	164
Nb	7·7	5·5	8·6	—	9·5	—	—	7·1
Mo	1·20	0·67	1·20	—	1·21	—	—	1·66
Sn	1·37	1·60	1·18	—	1·16	—	—	1·35
Sb	0·33	0·08	0·13	—	0·15	—	—	—
Cs	0·28	0·18	0·93	—	0·77	—	—	1·75
La	12·7	12·5	13·9	—	16·0	—	—	19·2
Ce	31·0	26·7	35·0	—	40·3	—	—	44·1
Pr	4·26	4·23	5·02	—	5·35	—	—	5·83
Nd	19·0	19·0	22·2	—	24·3	—	—	24·9
Sm	4·18	4·35	5·09	—	5·48	—	—	5·57
Eu	1·59	1·58	1·72	—	1·86	—	—	1·75
Gd	4·26	4·38	4·84	—	5·29	—	—	5·17
Tb	0·76	0·86	0·84	—	0·96	—	—	0·76
Dy	4·31	4·92	4·61	—	5·27	—	—	4·80
Ho	0·73	0·94	0·75	—	0·87	—	—	0·96
Er	2·05	2·60	2·06	—	2·45	—	—	2·77
Tm	0·28	0·38	0·29	—	0·33	—	—	0·40
Yb	1·89	2·54	1·87	—	2·22	—	—	2·54
Lu	0·27	0·37	0·28	—	0·33	—	—	0·37
Hf	2·70	3·32	3·76	—	4·22	—	—	3·91
Ta	0·45	0·35	0·54	—	0·60	—	—	0·41
Tl	0·04	0·03	0·15	—	0·10	—	—	—
Pb	7·21	7·29	9·15	—	5·26	—	—	6·96
Th	1·41	1·32	1·85	—	2·05	—	—	3·71
U	0·37	0·32	0·53	—	0·57	—	—	0·84
TIMS isotope ratios								
$^{87}Sr/^{86}Sr$	0·70613	0·70616	0·70660	0·70638	0·70539	0·70532	0·70567	0·70569
$^{143}Nd/^{144}Nd$	0·51277	0·51280	0·51277	0·51279	0·51280	0·51283	0·51263	0·51264
εNd	2·60	3·18	2·59	—	3·17	—	—	—
$^{206}Pb/^{204}Pb$	18·319	18·333	18·362	—	18·363	—	—	—
$^{207}Pb/^{204}Pb$	15·566	15·567	15·562	—	15·569	—	—	—
$^{208}Pb/^{204}Pb$	38·503	38·505	38·494	—	38·469	—	—	—

Table 2: Representative results of norm calculations for the Ueno Basalt lavas

Sample:	TKY1A	SZR1A	OHR3	TKT2B	KYM5B	KYZB	KZP2A	HSNB	TKKB	SKS1E	ATR1A	UGU1B	TNG
wt %													
SiO_2	51·27	50·65	51·64	45·99	52·01	47·33	49·45	50·52	49·57	49·55	51·75	52·36	49·08
TiO_2	1·13	1·11	1·10	2·32	1·27	1·45	1·57	1·46	1·21	1·26	1·28	1·23	1·61
Al_2O_3	16·39	16·50	16·21	15·23	17·78	14·43	15·61	15·69	15·64	14·95	16·65	17·30	17·47
Fe_2O_3	1·75	1·89	1·62	2·22	1·90	2·10	1·79	1·80	1·86	1·77	1·64	1·69	1·69
FeO	8·97	9·00	7·52	10·09	8·65	9·95	8·00	8·14	8·73	7·83	7·41	7·64	7·77
MnO	0·18	0·23	0·16	0·20	0·24	0·18	0·17	0·17	0·16	0·18	0·16	0·17	0·17
MgO	7·52	6·79	8·36	7·47	3·86	10·00	7·99	7·39	8·62	9·04	6·40	5·49	7·61
CaO	8·99	9·01	8·92	9·48	9·34	9·00	9·54	8·38	8·66	9·93	8·68	8·62	9·18
Na_2O	2·90	3·01	2·75	3·30	3·01	2·69	2·90	3·42	2·91	2·67	3·33	3·54	3·16
K_2O	0·73	0·67	0·68	0·73	1·31	0·70	0·78	0·88	0·70	0·82	0·75	0·79	0·59
P_2O_5	0·30	0·32	0·28	1·08	0·34	0·38	0·56	0·47	0·37	0·29	0·42	0·46	0·50
Total	100·13	99·17	99·25	98·12	99·69	98·19	98·36	98·32	98·43	98·28	98·47	99·28	98·82
Mg-no.	56·0	53·0	62·4	52·4	39·9	60·1	59·7	57·5	59·6	63·1	56·2	51·6	59·4
Σalkali	3·63	3·68	3·44	4·03	4·32	3·39	3·68	4·30	3·61	3·49	4·08	4·33	3·75
CIPW norm													
q	—	—	—	—	1·73	—	—	—	—	—	0·39	0·76	—
pl	54·03	55·50	53·52	53·19	56·78	48·87	52·69	54·69	53·02	49·86	57·36	59·34	59·21
or	4·31	3·96	4·08	4·37	7·74	4·20	4·67	5·32	4·20	4·90	4·49	4·73	3·49
ne	—	—	—	0·19	—	—	—	—	—	—	—	—	—
di	10·72	10·82	10·19	12·79	10·89	14·05	13·53	11·31	10·74	17·25	9·97	8·90	8·63
hy	21·92	20·53	27·01	—	16·90	6·98	15·05	14·91	16·81	12·60	21·90	20·40	12·07
ol	3·65	3·56	0·05	19·12	—	19·12	7·06	7·17	9·28	9·66	—	—	9·85
il	2·15	2·13	2·11	4·50	2·41	2·79	3·04	2·83	2·34	2·43	2·47	2·36	3·10
mt	2·54	2·77	2·36	3·28	2·77	3·10	2·64	2·65	2·74	2·61	2·42	2·46	2·48
ap	0·70	0·74	0·67	2·55	0·79	0·88	1·32	1·11	0·88	0·70	1·00	1·07	1·18
Suite	SAB	SAB	SAB	AB	SAB	TRB	SAB	SAB	SAB	SAB	SAB	SAB	SAB

The most silica-poor lavas were selected from each center. Ferric/ferrous ratio was calculated using the MELTS (Ghiorso & Sack, 1995) program by assuming magma generation conditions at the nickel–nickel oxide (NNO) buffer, 0·5 GPa, 1200°C. Mg-number as Mg/(Mg + Fe) molar ratios. AB, alkali basalt, SAB, sub-alkaline basalt, TRB, transitional basalt.

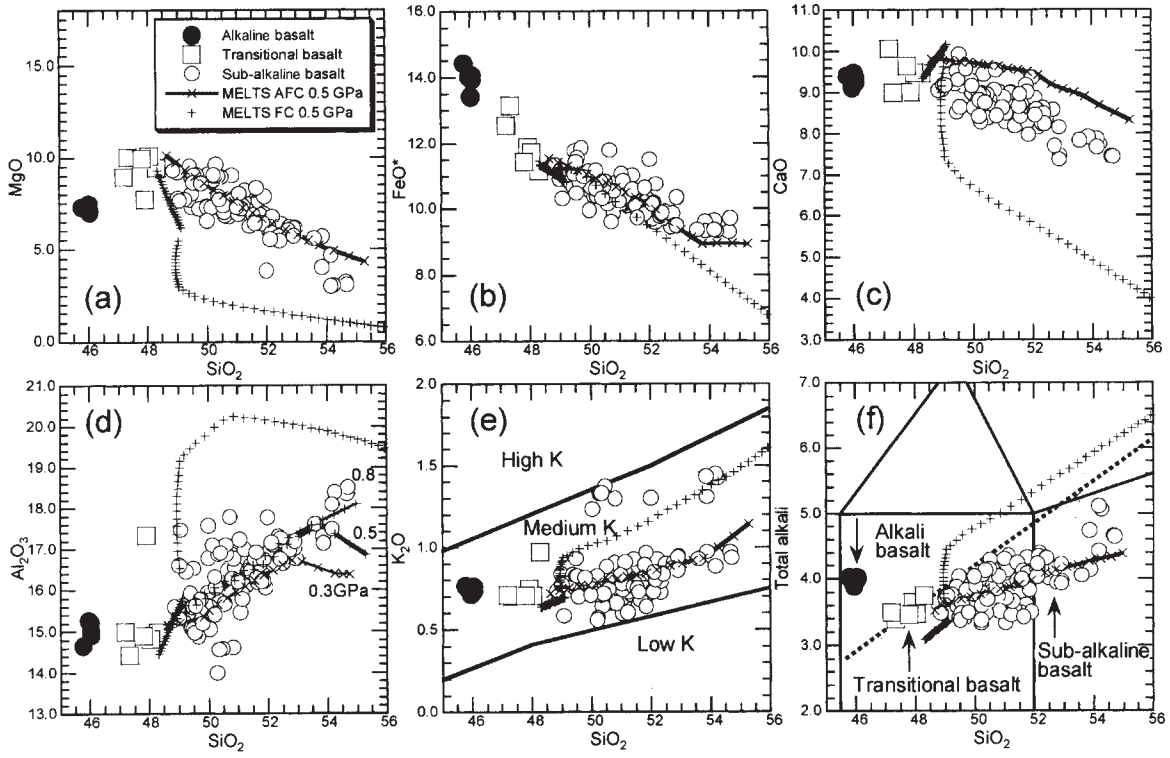

Fig. 3. Major oxide compositions (wt %) of the Ueno Basalts. Alkali basalts from Takataruyama have high alkali contents. Most other lavas are classified as basalt to basaltic andesite (Le Maitre *et al.*, 1989). Further classification is made in relation to the alkali and sub-alkaline boundary (Miyashiro, 1978) although an evolved lava from Takataruyama and a basalt from Kitazawa are transitional between alkali and sub-alkaline basalts. Notwithstanding these chemical differences, K_2O contents of all lavas are similar and define a medium-K suite. A fractional crystallization (FC) model for sub-alkaline basalt using MELTS (Ghiorso & Sack, 1995) is also shown (+); trend modeled at 0·5 GPa with H_2O = 1% deviates from that of the Ueno lavas. An AFC model (bold continuous lines) reproduces the Ueno chemical trend well (see text for discussion). Boundary lines are from Rollinson (1993) for K_2O, and from Miyashiro (1978) (dotted line) and Le Maitre *et al.* (1989) (continuous lines) for the total alkali–silica diagrams.

except for K/Rb, suggesting different sources. However, ranges of LILE ratios are highly variable, and overlap between the two groups.

The Ueno Basalt lavas have high REE contents, with steeper REE patterns in alkali basalts [$(Ce/Yb)_n \sim 8$]. Sub-alkaline basalts have lower REE contents and REE patterns are somewhat flatter [$(Ce/Yb)_n \sim 3{\cdot}5$] (Fig. 4a and b). Slight Ce anomalies (Ce/Ce* = 0·80–1·13; Table 1) are seen in some lavas. Eu anomalies are not obvious (Eu/Eu* = 0·97–1·15; Table 1), but lavas with slightly positive Eu anomalies are common among the basaltic andesites. This may reflect moderate plagioclase accumulation or contamination of mantle-derived melts by lower-crustal material (Taylor & McLennan, 1985). Evolved alkali basalts have characteristics intermediate between alkali and sub-alkaline basalts. Transitional basalts cannot be distinguished from sub-alkaline basalts on the basis of REE.

La/Yb ranges from 10 to 15 for alkali basalts and from 5 to 10 for sub-alkaline basalts (Fig. 5a). Alkali basalt La/Yb is similar to that of WPB (Sun & McDonough, 1989), and sub-alkaline basalt La/Yb falls between mid-ocean ridge basalt (MORB) and WPB ratios. The oldest alkali basalt (TKT2A) possesses the highest La/Yb, suggesting residual garnet in the mantle source. Transitional basalt La/Yb values are comparable with those of sub-alkaline basalts. Ba/Th ranges from 70 to 150 (Fig. 5b), comparable with the range of typical back-arc basalts (Turner *et al.*, 1998) or WPB suites (e.g. Samoa: Turner *et al.*, 1997). Nb/La reflects depletion of HFSE relative to LILE. Although Rb and K abundances in Ueno alkaline basalts are anomalously low, abundances of other incompatible elements are typical for alkali basalts. Nb/La for the alkali basalts is high (Nb/La = 0·9–0·95) whereas that of the sub-alkaline basalts is more variable and is lower by a factor of up to two (Nb/La = 0·6–0·35) (Fig. 5c). Transitional basalts are intermediate between the two suites or similar to alkali basalts (Nb/La = 0·6–0·75). Nb/La correlates with La, so the difference between the suites coincides with REE variations. Estimated Nb/La of primordial mantle is 0·87–1·42 (average Nb/La ~ 1) (Wood *et al.*, 1979; Thompson, 1982; Taylor & McLennan, 1985; Sun & McDonough, 1989). Nb/La for ocean island basalt (OIB) and MORB

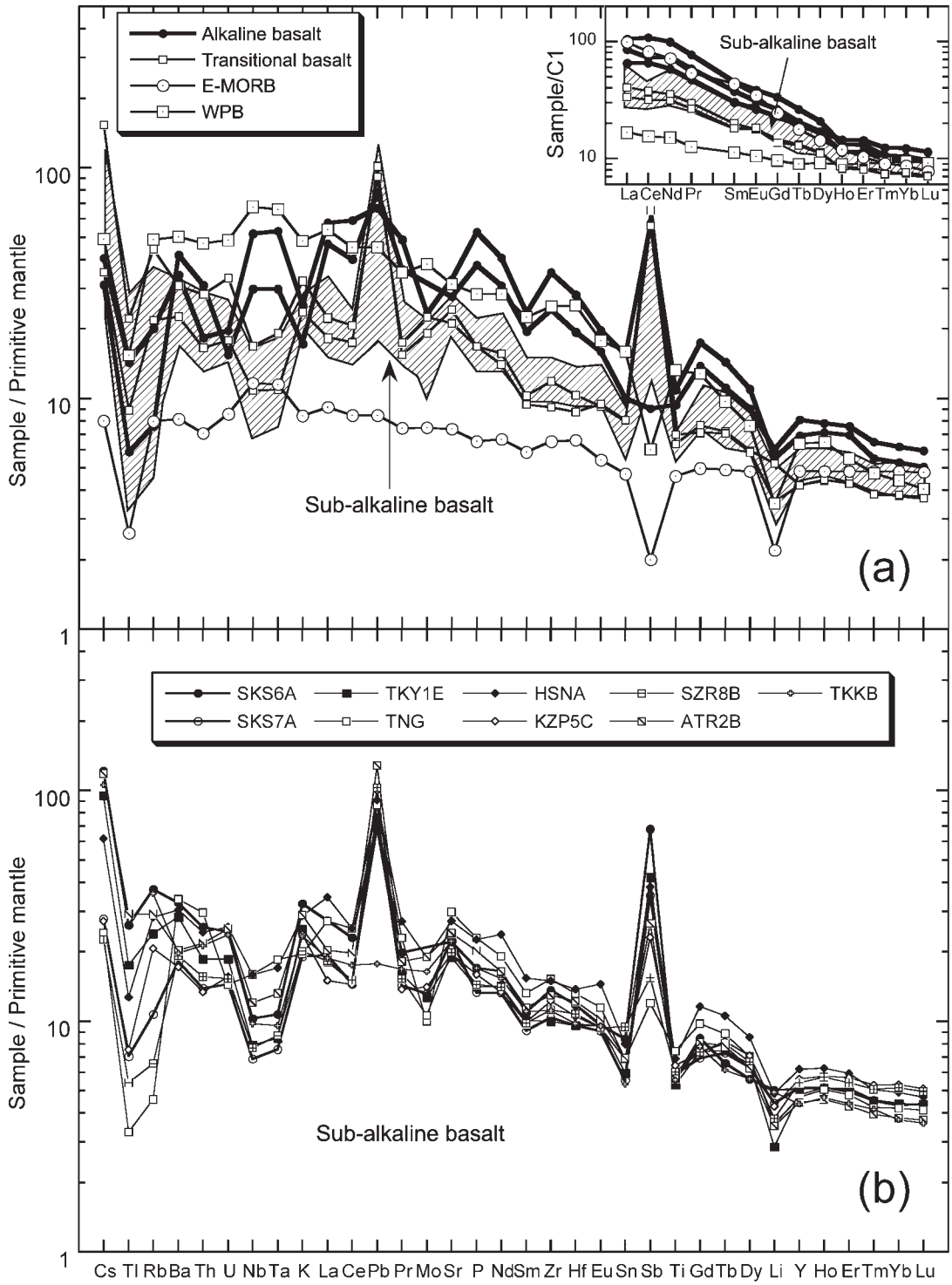

Fig. 4. Primitive mantle-normalized (Sun & McDonough, 1989) trace element variation diagrams for the Ueno Basalts. (a) Comparison of typical patterns for Ueno alkali basalts, Ueno transitional basalts, and field (diagonal lines) for Ueno sub-alkaline basalts [from (b)] with typical patterns for E-MORB and within-plate basalt (WPB); inset shows REE patterns, normalized to C1 chondrite abundances (Sun & McDonough, 1989). (b) Patterns for Ueno sub-alkaline basalt. Alkali basalts have patterns similar to WPB, including positive anomalies for Nb and Ta, whereas transitional and sub-alkaline basalts show patterns more similar to those of island-arc basalts (IAB), including Nb and Ta depletions. Positive Pb and Sb anomalies occur in most samples. Cs, Rb, U, and K contents are similar for all Ueno Basalts.

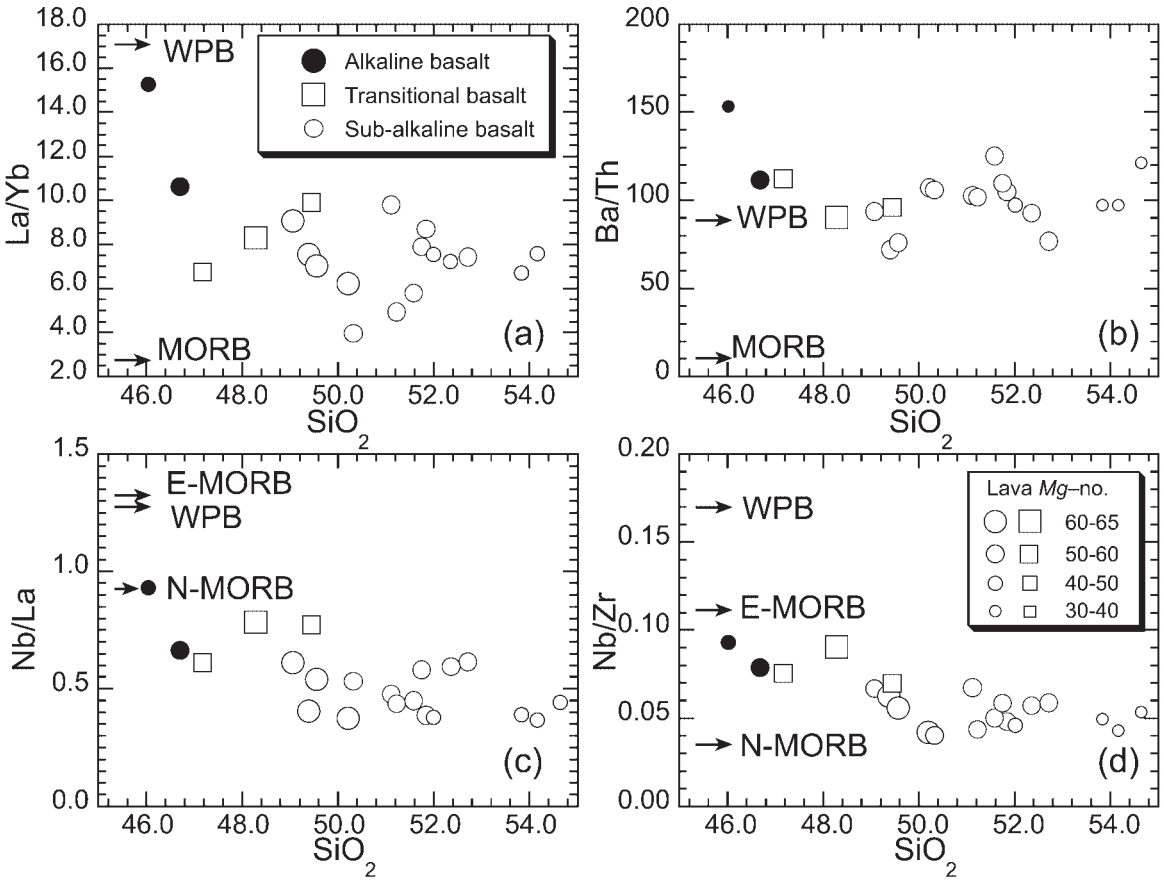

Fig. 5. Incompatible trace element ratios vs wt % SiO_2 for the Ueno Basalt lavas. La/Yb (a) for the most silica-poor alkali basalt is high compared with that of sub-alkaline and transitional basalts. Ba/Th (b) is low, suggesting a minor contribution of fluids derived from the subducted slab. The Nb/La diagram (c) shows the greater depletion of high field strength elements in the sub-alkaline basalts. Nb/Zr (d) is high for alkali and transitional basalts and low for sub-alkaline basalts. WPB and MORB ratios are from Sun & McDonough (1989).

are 1·5 and 0·83, respectively (Saunders & Tarney, 1984). The Nb/La ratios of Ueno alkali basalts are similar to those of OIB and fertile mantle, whereas sub-alkaline basalt Nb/La ratios are low and compare with continental crust or N-MORB (Nb/La = 0·68) (Weaver & Tarney, 1984; Taylor & McLennan, 1985).

Nb/Zr monitors HFSE fractionation (Fig. 5d), and ranges from 0·03 to 0·1 in the Ueno basalts intermediate between MORB (0·03) and WPB (0·17) (Sun & McDonough, 1989). As a result of high Zr contents, Ueno alkali basalts have lower Nb/Zr than typical WPB. Nb/Ta of the alkali basalts is higher (18–19) relative to that of the sub-alkaline basalts (15–18). The Nb/Ta ratios of the sub-alkaline basalts compare with the chondrite value inferred for global reservoirs (Nb/Ta = 17; Green, 1995), such as MORB or WPB, but are still within the range of island-arc lavas (Green, 1995; Münker, 1998).

Isotopic compositions

$^{87}Sr/^{86}Sr$ ranges from 0·7045 to 0·7076 (Fig. 6a), which is high relative to volcanoes in the Shinetsu Mountains (0·7035), located on the Pacific Ocean side of central Japan (Kaneko, 1995). $^{87}Sr/^{86}Sr$ values of Ueno Basalts compare more closely with those in the Hakusan Volcanic Chain (0·705–0·706; Notsu *et al.*, 1989) and in the southern part of the Tohoku–Honshu arc (0·706–0·715; Kersting *et al.*, 1996). The most MgO-rich lava from the Kitazawa center (Fig. 1b) has the lowest $^{87}Sr/^{86}Sr$ among Ueno Basalts (Fig. 6b). Fractionated sub-alkaline basalts generally have more radiogenic Sr-isotope compositions. Alkali basalt lavas generally have lower $^{87}Sr/^{86}Sr$ than the sub-alkaline basalts.

Nd isotopic compositions ($^{143}Nd/^{144}Nd$) of the Ueno Basalts vary from 0·51251 to 0·51290 ($\varepsilon Nd = -2{\cdot}5$ to 5·1), showing similar diversity to the Sr isotopic compositions (Fig. 6a). This range is similar to that found for all lavas from the entire southern Tohoku–Honshu arc (Kersting *et al.*, 1996). Transitional Kitazawa lavas are isotopically similar to alkali basalt lavas ($\varepsilon Nd = 5{\cdot}0$). The most SiO_2-poor alkali basalt has the highest $^{143}Nd/^{144}Nd$ (Fig. 6b). Most sub-alkaline basalts are isotopically similar to the Kitazawa lava, but increasing SiO_2 is

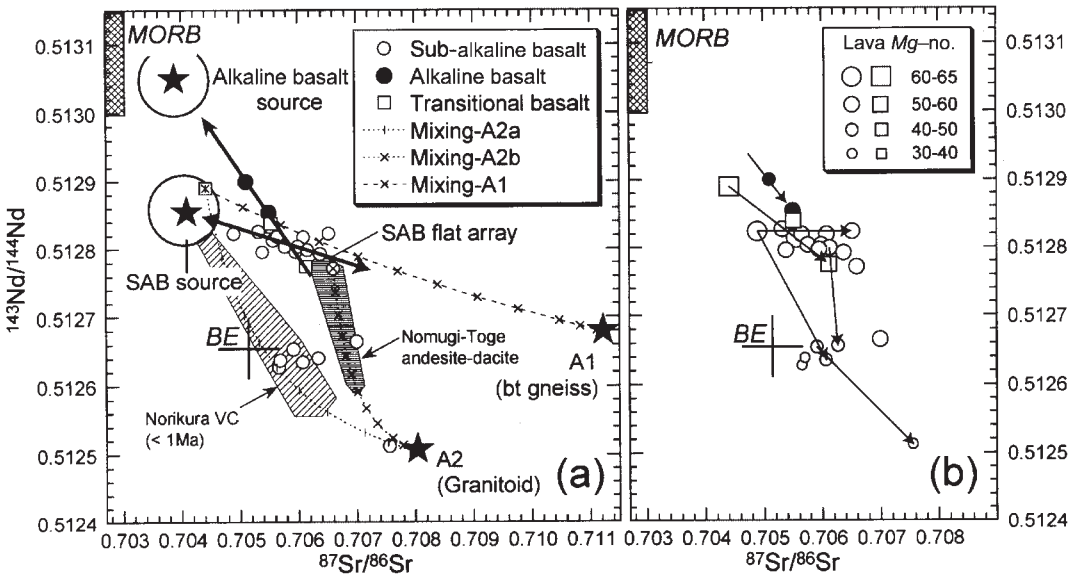

Fig. 6. $^{143}Nd/^{144}Nd$ vs $^{87}Sr/^{86}Sr$ for the Ueno Basalts. Alkali basalts have the highest $^{143}Nd/^{144}Nd$; among the sub-alkaline basalts, true basalts (SiO_2 <52 wt %) plot on a flat array (shown as 'SAB flat array': bold line with arrows), whereas basaltic andesites have lower $^{143}Nd/^{144}Nd$. Stars with mixing lines A1 (Hida biotite gneiss: Tanaka, 1992) and A2 (weighted average of basement granitoids: Tanaka, 1992) are possible crustal contaminants for the Ueno lavas. Fine connecting lines with small arrows show lava pairs from single centers (arrows show increasing SiO_2). The most magnesian alkali basalts plot at the upper left end of the alkali basalt array. Source compositions for the suite should lie on the extrapolated line (continuous bold arrow). The most magnesian sub-alkaline basalt has a source composition between MORB and Bulk Earth 'BE' (Zindler & Hart, 1986) (shown as filled star with circle). Norikura VC indicates basalt and andesite lavas younger than 1 Ma from the Norikura Volcanic Chain (J.-I. Kimura, unpublished data, 1999; Ujike & Stix, 2000); Nomugi-Toge indicates andesite to dacite lavas from the Nomugi–Toge Volcanic Rocks (J.-I. Kimura, unpublished data, 1999).

accompanied by decreasing $^{143}Nd/^{144}Nd$. Basaltic andesites from the Takayama, Sakashita, and Kiyomi centers have lower $^{143}Nd/^{144}Nd$ and a larger range in isotopic compositions.

In Nd–Sr isotope space, the Ueno Basalts plot to the right of the MORB–Bulk Earth join (Fig. 6). The most MgO-rich transitional Kitazawa samples are intermediate between MORB and Bulk Earth (Zindler & Hart, 1986). In contrast, most sub-alkaline Ueno lavas scatter to the right (Fig. 6a and b). Sub-alkaline basalts have high $^{143}Nd/^{144}Nd$ and form a flat array (see SAB flat array in Fig. 6a). Trends defined by basalts and basaltic andesites from the Takayama, Sakashita, and Kiyomi sub-alkaline centers are highly oblique to the SAB flat array. These differing isotopic trends suggest that at least three mixing end-members exist for the sub-alkaline basalts. Alkali basalts commonly have higher $^{143}Nd/^{144}Nd$ than sub-alkaline lavas, and a smaller range. Variations within the alkali basalt suite are oblique to the SAB flat array, and the most silica-poor alkali lava plots at the depleted end of the trend. The source for the primary alkali basalt may have higher $^{143}Nd/^{144}Nd$ than this, because even the most silica-poor alkali basalt is fractionated (and potentially contaminated). The most primitive transitional basalt from Kitazawa is intermediate between the alkali basalts and the SAB flat array, and tie lines between this and more evolved lavas lie sub-parallel. Other transitional basalts plot on a linear array together with the alkali basalts (Fig. 6a).

$^{206}Pb/^{204}Pb$ of the Ueno Basalts ranges from 18·31 to 18·43, $^{207}Pb/^{204}Pb$ = 15·54–16·2, and $^{208}Pb/^{204}Pb$ = 38·39–38·84 (Fig. 7a–c; Table 1). $^{207}Pb/^{204}Pb$ and $^{208}Pb/^{204}Pb$ ranges approximate those reported from the Tohoku–Honshu arc (Kersting *et al.*, 1996; Shibata & Nakamura, 1997), but $^{206}Pb/^{204}Pb$ is lower and comparable with values for basalts from Tohoku–Honshu back-arc volcanoes or from Hokkaido back-arc basin basalt (Shibata & Nakamura, 1997; Okamura *et al.*, 1998). The $^{208}Pb/^{204}Pb$ plot clearly shows that the Ueno basalts have isotopic characteristics of the DUPAL anomaly (Hart, 1984) and belong to the Indian Ocean domain (Flower *et al.*, 2001) together with NE Honshu and SW Japan basalts. However, these features may have originated by addition of subducted material or by assimilation of lithosphere.

Pb isotope compositions of Ueno Basalts define a linear trend, which extends between fields for Pacific MORB

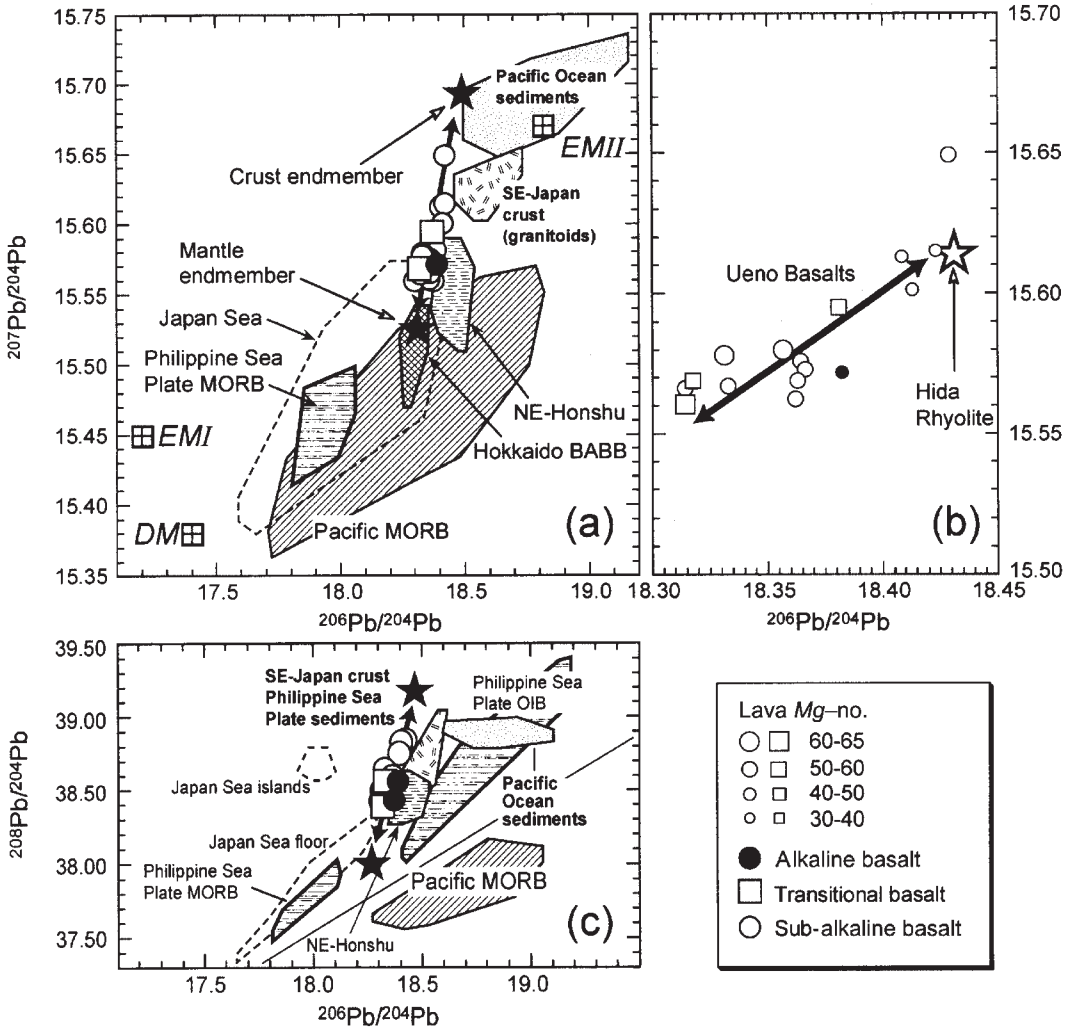

Fig. 7. Plot of $^{207}Pb/^{204}Pb$ vs $^{206}Pb/^{204}Pb$ for the Ueno Basalts (a, b). (c) $^{208}Pb/^{204}Pb$ vs $^{206}Pb/^{204}Pb$. The lavas plot on a trend (bold line with arrows) together with possible crustal melts of the Hida Rhyolite (Kimura *et al.*, 1999). The most silica-deficient sub-alkaline basalt, alkali basalt, and transitional basalt lavas all plot close to the low $^{206}Pb/^{204}Pb$ end of the array. In contrast, the most silica-rich Kiyomi sample plots at the high $^{206}Pb/^{204}Pb$ end. Assumed crustal contaminant(s) should approach EMII compositions, whereas the mantle end-member may lie close to the MORB or Sea of Japan fields. EMI, enriched mantle I; EMII, enriched mantle II; DM, depleted mantle (Zindler & Hart, 1986). Data from SE Japan granitoids and Pacific Ocean sediments (Shimoda *et al.*, 1998), Tohoku lavas (Kersting *et al.*, 1996; Shibata & Nakamura, 1997), Hokkaido back-arc basin basalts (BABB) (Okamura *et al.*, 1998), the Japan Sea and East China lavas (Pouclet *et al.*, 1995), and the Philippine Sea plate MORB from Shikoku–Parece Vela (Hickey-Vargas *et al.*, 1995).

and an enriched reservoir that could be EMII, Pacific sediments, or Japanese continental crust (Fig. 7a and c). The most magnesian Kitazawa basalt plots at the end of the trend close to the Pacific MORB field, whereas the most MgO-poor lava from Kiyomi plots at the most enriched end. Alkali basalts show similar ratios to that of Kitazawa, but plot slightly to the high-μ side (Fig. 7b). The most depleted ends of the basalt suites, together with back-arc lavas from Hokkaido, fall within the field defined by lavas from the Japan Sea (Pouclet *et al.*, 1995). The Shikoku–Parece Vela–Philippine Sea plate MORB (Hickey-Vargas *et al.*, 1995) is isotopically distinct from the Ueno lavas, suggesting no contribution from the subducting Philippine Sea slab beneath the area.

DISCUSSION

Ueno Basalts are variable in terms of both trace element abundances and isotopic compositions. Incompatible trace element concentrations vary from those similar to WPB-type alkali basalt to typical IAB-type sub-alkaline basalt. Isotopic compositions are also highly variable, with a range that is comparable with the variation shown by the entire Tohoku–Honshu arc. These variations

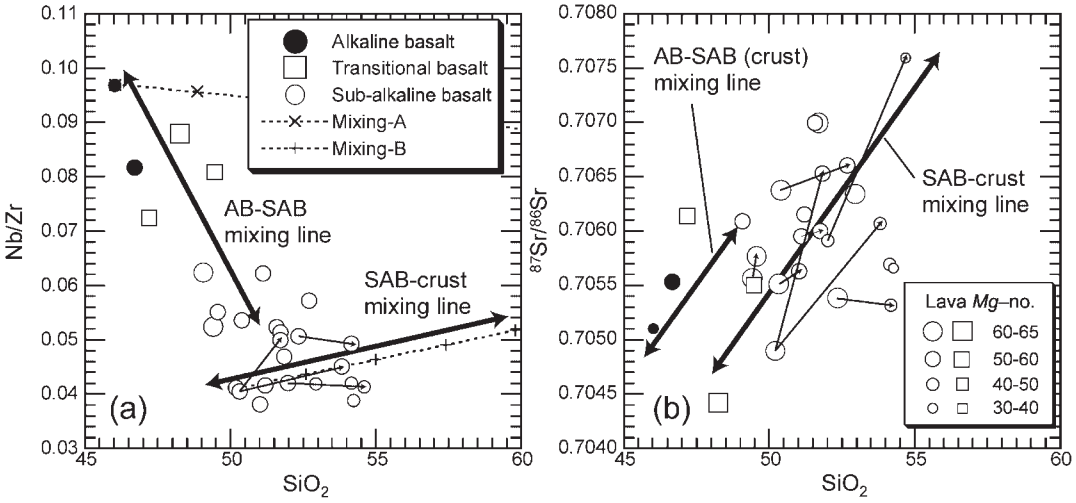

Fig. 8. Plot of wt % SiO_2 vs (a) Nb/Zr and (b) $^{87}Sr/^{86}Sr$ for the Ueno Basalts. Fine lines connect lavas from individual centers. Sr isotope ratios covary with increasing SiO_2 in the sub-alkaline suite. The same is true between pairs of silica-poor and silica-rich lavas from single centers, suggesting that crustal contamination was an important part of magma evolution (Kimura & Yoshida, 1999). Alkali basalts show relatively modest increases in $^{87}Sr/^{86}Sr$ with increasing silica. Nb/Zr differs greatly between alkali and sub-alkaline suites, and there is a small range of variation in Nb/Zr within the sub-alkaline lavas. Alkali–transitional basalt arrays in both figures indicate mixing between alkali and sub-alkaline compositions (AB–SAB mixing line), whereas the trend observed for the sub-alkaline suite indicates that crustal contamination is important (SAB–crust mixing line).

could reflect mantle heterogeneity, crustal contamination, or both.

In the sub-alkaline basalt suite, Sr, Nd and Pb isotopic ratios covary with major elements (e.g. Fig. 8b). This variation is apparent for both the entire sub-alkaline basalt suite as well as for individual eruption centers. Sr isotope ratios are higher in SiO_2-rich alkali basalts. Fractional crystallization alone cannot affect isotopic compositions or incompatible trace element ratios, particularly in basalt suites, as shown by a Nb/Zr vs SiO_2 plot (Fig. 8a). This figure strongly suggests mixing between alkali basalt and sub-alkaline basalt and mixing between sub-alkaline basalt and a crustal contaminant. Increasingly radiogenic Sr isotopic compositions with increasing silica can be explained by progressive crustal contamination of melts during magma ascent (Davidson, 1996). Silica enrichment in the source mantle peridotite may also be caused by addition of silica-rich slab melts to the sub-arc mantle (Kelemen *et al.*, 1998), which may also cause isotopic enrichment. In the following discussion, we outline why we conclude that crustal contamination is the principal cause of variation in the Ueno sub-alkaline basalts' incompatible element ratios and isotopic compositions, and how the source mantle differs.

Origin of the Ueno Basalts

Evidence for crustal assimilation in sub-alkaline suite lavas

Sharp decreases in MgO (from 10 to 3 wt %) accompany increasing SiO_2 in the sub-alkaline Ueno basalt suite (see Fig. 3a). In this compositional range, lavas vary from olivine basalt to olivine–cpx basalt to plagioclase-bearing olivine–cpx basaltic andesite as silica increases (Kimura & Yoshida, 1999), suggesting a role for low-pressure fractional crystallization. A strong variation in isotopic composition accompanies fractionation, and this is attributed to crustal contamination of the evolving magmas. Clinopyroxene–melt geothermobarometry (Putirka *et al.*, 1995) suggests that the Ueno lavas resided at pressures between 0·7 and 1·3 GPa for some time before eruption (Kimura *et al.*, 1999). This corresponds to depths of the middle crust to the uppermost mantle in this area (Zhao *et al.*, 1992).

A major element assimilation–fractional crystallization (AFC) model was developed using the most Mg-rich (MgO ~10 wt %) sub-alkaline basalt from Takakurayama (TKKA and TKKB) as a starting composition and a silicic crustal melt as the contaminant (Table 3) (Ghiorso & Sack, 1995). The assimilated weight of silicic melt is set at 30% of the original basalt weight for basalt to basaltic andesite compositions (SiO_2 composition up to 55 wt %) based on mixing proportions deduced from the biotite gneiss and the Kitazawa (or Takakurayama) isotope mixing model (see Fig. 6a). Plausible crustal contaminants should be siliceous, to cause increase in silica in the sub-alkaline basalt suite. In the first step, a silica-rich rhyolite ignimbrite of the Hida Volcanic Rocks (Kimura *et al.*, 1999), of the same age as the Ueno Basalt, was chosen as the contaminant. One discrepancy occurs between the calculated composition and the sub-alkaline basalt chemistry. The rhyolite is very potassic, which

Table 3: Chemical compositions of primitive sub-alkaline basalt (SAB) and crustal contaminant used in MELTS (Ghiorso & Sack, 1995) calculations

Element	Primary SAB	Contaminant
SiO_2	48·64	76·42
TiO_2	1·52	0·18
Al_2O_3	15·17	16·49
Fe_2O_3	1·71	0·65
FeO	8·93	1·39
MnO	0·18	0·06
MgO	10·12	0·03
CaO	9·82	1·25
Na_2O	2·81	2·49
K_2O	0·72	1·03
P_2O_5	0·39	0·01
Total	100·00	100·00
Fe^{2+}/Fe^{3+} calc.	NNO	QFM + 1

Ferric/ferrous ratios were calculated at NNO and QFM (quartz–fayalite–magnetite) + 1 buffer conditions using the MELTS program. The crustal contaminant was set at 850°C and progressively added at a constant rate until 30 wt % of basalt finally mixed at melt composition SiO_2 55 wt %. Contaminant is the K_2O-adjusted high-silica rhyolite ignimbrite.

causes significant increase in K_2O during assimilation. The K_2O value was therefore adjusted to a more appropriate composition, as shown in Table 3. This simple adjustment makes the model fit almost all major element compositions, and evolved lava compositions [e.g. the Sakashita (SKS1D)], are reproduced well. Modeled CaO and TiO_2 are slightly higher than observed for sub-alkaline lavas. The low-K, high-silica crustal composition also resembles melts produced by hornblende dehydration melting (Johannes & Holtz, 1996). This is consistent with the expected stability of amphibolite facies rocks in the middle to lower crust.

$^{87}Sr/^{86}Sr$ ratios of basement granitoids and gneiss range from 0·7045 to 0·710 and $^{143}Nd/^{144}Nd$ ratios of the basement rocks vary from 0·5119 to 0·5129 (Arakawa, 1990; Tanaka, 1992). Most basement rocks have higher $^{87}Sr/^{86}Sr$ and lower $^{143}Nd/^{144}Nd$ than the Ueno Basalts, and are therefore plausible contaminants of mantle-derived Ueno mafic melts. For example, Hida biotite gneiss (Tanaka, 1992) could explain some samples in the sub-alkaline basalt (SAB) flat array (Fig. 6a). Compared with Ueno Basalts, this gneiss has much more radiogenic $^{87}Sr/^{86}Sr$ but similar $^{143}Nd/^{144}Nd$. Basement granitoids are also possible contaminants for the vertical low $^{87}Sr/^{86}Sr$ array of the sub-alkaline suite, because the former rocks have much higher $^{87}Sr/^{86}Sr$ and lower $^{143}Nd/^{144}Nd$ than the Ueno Basalts. A hypothetical contaminant is estimated from the average isotopic composition of these granitoids. Model mixing calculations were made between the most magnesian Ueno lava (Kitazawa or Takakurayama) and these two potential contaminants (mixing models A1 and A2 in Fig. 6). Mixing model A1 reproduces the SAB flat array isotope trend. Mixing model A2a fits well with the low Nd trend of the evolved Ueno lavas, which is represented by evolved Sakashita, Kiyomi, and Takayama lavas (see evolved–less evolved sample joins in Fig. 6b), except that the proportion of contaminant is high. The high mixing proportion reflects the choice of hypothetical contaminant compositions. However, the isotopic characteristics of the basement granitoids are commonly similar to an EMII component so the general tendency is adequate. Mixing between the A2 granitoid and the radiogenic Sr end of the SAB flat array (mixing model A2b) also fits well with other Ueno sub-alkaline basalts represented by a join between evolved and less evolved Takayama samples (Fig. 6b). This suggests that two stages of mixing may have taken place for some evolved Ueno lavas, first with the A1 gneiss end-member and then with the A2 granitoid end-member. These A2a and A2b mixing lines are parallel to the isotopic variations of younger (<1 Ma) intermediate lavas from the Norikura Volcanic Chain (A2a) and the Nomugi–Toge andesite–dacite (the same age as the Ueno; A2b) (Fig. 6a). This indicates that intermediate lavas in the Norikura Volcanic Chain are the products of mixing between upper-crustal granitoid and Ueno-like basalts that had already assimilated an A1 gneiss component to various degrees. Geobarometry indicates that assimilation occurred at lower-crustal depths (1·3 GPa), with biotite gneiss (A1) characterizing the lower crust, whereas granitoid (A2) characterizes the middle crust (0·7 GPa). It is notable that isotopically depleted alkali basalt (Takataruyama), transitional basalt (Kitazawa), and magnesian sub-alkaline basalts (Takakurayama) are all located in the center of the Ueno Basalt Province. In contrast, highly contaminated lavas, such as Sakashita, Kiyomi, and Takayama, occur at the perimeter.

Pb isotope data are not available for potential basement contaminants. However, the most siliceous Ueno Basalts have the most radiogenic Pb isotopic compositions and have similar isotopic compositions to the Hida Rhyolites. The Hida Rhyolites are thought to have formed by mixing between crustal melts and a basaltic magma (Kimura *et al.*, in preparation), suggesting that crustal contaminants have even more radiogenic Pb. A plot of $^{207}Pb/^{204}Pb$ vs $^{206}Pb/^{204}Pb$ (Fig. 7a and c) shows that the most radiogenic end of the Ueno Basalt trends is similar

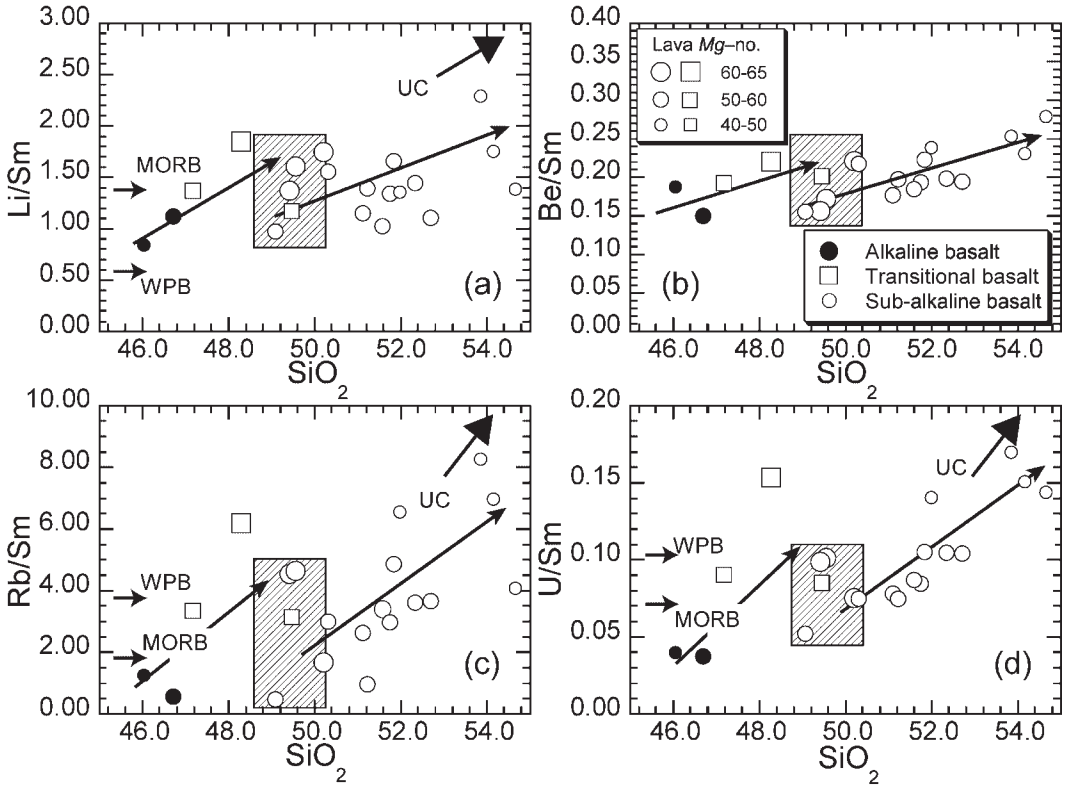

Fig. 9. Correlation of wt % SiO_2 vs ratios of various fluid mobile elements (FME) with respect to MREE (Sm) for the Ueno Basalts. All FME/MREE ratios covary with SiO_2 in the sub-alkaline (SAB) suite and coincide with isotopic enrichment of these lavas (Fig. 8), suggesting progressive contamination of FME through AFC processes. Estimated primary SAB compositions (diagonal ruled squares) and AFC trends (unlabeled arrows with small arrowheads) are shown. Alkali basalt FME/MREE are about half those of primary SAB, suggesting that fluid mobile element abundances are similar in both sources, because Sm abundances in the alkali suite are almost half those in the sub-alkaline suite (Fig. 4). Enrichments of fluid mobile elements in the sub-alkaline basalts are attributed mostly to crustal contamination. Arrows labeled WPB and MORB indicate incompatible element ratios for WPB and E-MORB (Sun & McDonough, 1989). Arrows labeled UC, with large arrowheads, indicate upper continental crust SiO_2 and trace element values from Taylor & McLennan (1985).

to EMII or Pacific Ocean sediments. However, this end-member probably represents local crustal contaminants, as discussed above. Mino Zone granitoids in southwestern Japan have Pb isotopic compositions similar to EMII (Shimoda *et al.*, 1998) and to the radiogenic Ueno Basalt end-member. The most magnesian basalt from Takakurayama (TKKB in Fig. 4) has no positive Pb spike in a mantle-normalized trace element variation diagram, and has a depleted Pb-isotopic signature (see Fig. 7b). We thus consider that the large isotopic variations seen in the sub-alkaline Ueno Basalts reflect contamination by crustal materials.

Abundances of fluid mobile elements (FME) relative to middle REE (MREE) (Sm) can be used to identify the behavior of FME during magmatic processes (Fig. 9). Li/Sm, Be/Sm, Rb/Sm, and U/Sm increase with increasing SiO_2 and decreasing Mg-number in the sub-alkaline suite. The same is also true for K/Sm, Sb/Sm and Th/Sm (not shown). All trends are directed from MORB or WPB levels toward the composition of the upper continental crust (Taylor & McLennan, 1985) or an upper-crustal melt (e.g. the Hida Rhyolite) in this area (Fig. 9). This clearly shows that crustal assimilation not only affects isotopic and major element compositions but also affects FME, and thus arc basalt signatures. Less differentiated sub-alkaline basalts (low silica with high magnesium: see Fig. 9) always have low FME/MREE; therefore, the FME enrichment relates to isotopic EMII enrichment. These observations give an important indication that the FME enrichment found in the Ueno sub-alkaline suite is in part caused by crustal assimilation.

Overall, high-magnesian sub-alkaline basalts (e.g. Takakurayama), are less affected by crustal assimilation and may closely represent the melt composition produced by lithospheric mantle melting (see discussion below). Significant crustal assimilation is apparent in basaltic andesites from Sakashita and Kiyomi.

Evidence of mixing in the alkali basalt suite

The isotopic compositions of the alkali basalts vary little, and generally define a high-εNd end-member similar to MORB-source mantle (see Figs 6a and 7). Isotopic trends of the alkali to transitional basalt suites from the Takataruyama center lie between the flat array group of the sub-alkaline suite and MORB-like compositions (see Fig. 6a). Similar linear trends are also observed for major elements, which are again drawn between the most primitive alkali basalt and sub-alkaline basalt (see Fig. 3b–f). The same mixing feature is shown by both incompatible element ratios (Figs 5 and 8a) and FME/MREE (Fig. 9), where all but one of the transitional basalt samples plot between alkali basalt and primitive sub-alkaline suite lavas. Figure 8a, in particular, suggests that mixing between alkali and sub-alkaline basalts can produce transitional basalt, and that a crustal contaminant cannot be a mixing end-member for alkali basalt. Trends in major elements, trace elements and Sr–Nd–Pb isotopes all suggest mixing between primary alkali basalt and sub-alkaline basalt components, and that transitional basalt is a product of this mixing (see Figs 3, 6 and 7). Alkali and transitional basalts erupted at the beginning of Ueno volcanic activity (2·76–2·71 Ma for TKT and 2·72 Ma for KTZ). Alkali and sub-alkaline components should thus have existed contemporaneously, at least at the beginning of Ueno volcanism.

Mantle source for the Ueno Basalts

Two distinctive mantle sources for alkali and sub-alkaline basalts

As discussed above, alkali basalt lavas were derived from a distinct mantle source, isotopically similar to MORB (Fig. 6a). In contrast, sub-alkaline basalt (SAB) lavas were derived from an isotopically enriched source intermediate between MORB and Bulk Earth (Fig. 6a). These discrete mantle sources are discussed below.

Magma segregation depths

Primitive alkali and sub-alkaline magma compositions have been estimated (Kimura *et al.*, 1999) using progressive addition of fractionated minerals until magma compositions are in equilibrium with upper-mantle peridotite. Estimated magma segregation depths lie within the upper mantle: 1·5–2·5 GPa (~60 km deep) for sub-alkaline basalt and 2·5–3 GPa (~90 km deep) for alkali and transitional basalts [pressures using the basalt tetrahedra projection of Takahashi & Kushiro (1983)]. Magma chamber depths estimated by cpx–melt geobarometry (1·3–0·7 GPa) are much shallower than the inferred segregation depths.

La/Lu and Yb/Gd are principally controlled by source mantle mineralogy, particularly residual garnet during melting (Feigenson *et al.*, 1983; Caroff *et al.*, 1997); it is plausible that the Ueno alkali basalts originated from the garnet-lherzolite and the sub-alkaline basalts from the spinel-lherzolite stability fields. Garnet is estimated to be stable in the upper mantle at depths greater than 70–90 km (Green & Ringwood, 1967; Takahashi & Kushiro, 1983; Robinson & Wood, 1998). Pressure estimates from major elements are consistent with source mineralogy inferred from trace elements.

Degree of partial melting

Variations in the degree of melting can cause differences in incompatible element abundances, especially at small degrees of melting (e.g. Shaw, 1970). Abundances of incompatible elements in the alkali basalts are generally high, whereas those in the sub-alkaline basalts are low. For basalt compositions, the degree of melting can be estimated from an SiO_2–total alkali diagram (Kushiro, 1994). Using this method suggests that Ueno alkali basalt represents about $F = 7\%$ ($P > 2{\cdot}5$ GPa) and sub-alkaline basalt $F = 12\%$ ($P = 1{\cdot}5$ GPa). Degree of partial melting can also be estimated by using SiO_2 contents (wt %) calculated at 9 wt % MgO (Klein & Langmuir, 1987). The petrogenetic grid of Klein & Langmuir (1987) (their fig. 6) is not applicable for the alkali basalt; however, extrapolation of the dataset is used for F% estimates. Estimated degrees of melting are $F = 7\%$ for alkali basalt ($P = 3{\cdot}0$ GPa) and $F = 13\%$ ($P = 1{\cdot}5$ GPa) for sub-alkaline basalt, similar to the estimates based on the method of Kushiro (1994).

Chemical characteristics of alkali and sub-alkaline suite sources

Depletions in HFSE were shown with Nb/La, and these ratios differ between alkali and sub-alkaline basalt (Fig. 5c). This may reflect LILE-rich fluid or melt addition as a result of dehydration or melting of subducted crust and sediments (Davidson, 1996; Stolz *et al.*, 1996), or could be due to survival of residual HFSE-bearing minerals such as rutile (Green, 1995) or spinel (Bodinier *et al.*, 1996) during melting or source metasomatism. We here examine the chemical characteristics of the source.

Ba/Th has been used to estimate addition of fluid from the subducted slab to the mantle (Turner *et al.*, 1998). Ba/Th of the Ueno lavas is below 150 (Fig. 5b), comparable with WPB or a depleted mantle source, indicating that the mantle source for Ueno Basalt was not highly metasomatized by fluids. However, high abundances of fluid mobile elements (FME) such as Li, Be, Sb, and Pb (Bebout *et al.*, 1999) in the sub-alkaline basalts suggests some fluid addition or addition of these elements by crustal assimilation, and the causes must be

evaluated. As anhydrous mantle minerals may show small differences in D values for fluid mobile elements, we can discuss abundances of FME in alkali and sub-alkaline sources. The most primitive (SiO_2 49 wt %) sub-alkaline basalt has Ba/Th and FME/MREE ratios similar to those in the alkali basalt (SiO_2 46–47 wt %; Figs 5b and 9). As shown in Fig. 9, FME/MREE ratios are almost identical for primitive alkali basalt and sub-alkaline basalt. Mantle-normalized trace element variation diagrams show significant positive anomalies of Pb and Sb in sub-alkaline basalts (Fig. 4b). However, the lowest value for Pb is similar to those of neighboring elements. We conclude that the FMEs are largely added to the sub-alkaline basalt through crustal assimilation rather than by mantle metasomatism.

Concentrations of FME, such as Rb, K, U, and Th, are low in the alkali basalt and are comparable with or even lower than for the sub-alkaline basalts (see Figs 3 and 4). Ratios of FME/MREE in some alkali to transitional basalt lavas covary with SiO_2, suggesting that crustal assimilation is responsible (Fig. 9a, c and d). This, in turn, suggests very low abundances of these elements in the primary alkali basalt and in the mantle source itself, or that FME-bearing minerals were residual after partial melting. Relative K depletion can be modeled by a two-stage melting process, whereby a melt produced by a low degree of partial melting of mantle peridotite with minor residual amphibole and phlogopite in the garnet stability field metasomatized the overlying mantle, and the metasomatized mantle melted to produce the K-depleted basalts (Halliday *et al.*, 1995). The low FME concentration in the alkali basalts can be explained by this model.

Incompatible element concentrations in the alkali basalts are about 1·3–2·5 times higher than in the sub-alkaline basalts (except for HFSE, which are almost an order of magnitude higher in the alkali basalt; the reason for this will be discussed below). This difference can be achieved by differences in the degree of partial melting (F% = 15–6) in both batch and fractional melting models for most incompatible elements that have bulk D = 0·1–0·001 (Shaw, 1970). This estimate does not include differences in mineralogy for the two basalt sources. The presence of garnet in the alkali basalt source should enhance LREE/LILE in the alkali basalt at a given F. In this context, the alkali basalt source should be more depleted in FME than the sub-alkaline basalt source. Trace element variation diagrams (Fig. 4) show that the Ueno alkali basalts are depleted in LILE relative to WPB alkali basalts. The source mantle for the sub-alkaline basalt is thought to be enriched in FME relative to the alkali basalt source. The shallower sub-alkaline basalt mantle source is also enriched in terms of incompatible radiogenic isotopes such as Sr (see alkali basalt and SAB sources in Fig. 6a).

In addition to FME and REE, elevated abundances of HFSE in the alkali basalts are distinctive (Fig. 10a and b). However, a relatively small depletion in HFSE/REE in the primitive sub-alkaline basalts is also characteristic of the Ueno Basalts (Figs 4b and 10a), and the origins of this depletion should be examined. Nb/La and Nb/Zr correlate well with Tb/Lu (HREE/MREE) in the sub-alkaline basalt suite, consistent with mixing between primary sub-alkaline basalt and the assumed Hida Rhyolite crustal contaminant (Fig. 10a). It is noteworthy that Nb/La in the primary SAB is almost identical to N-MORB, and that the HFSE depletion becomes more pronounced by mixing with the crustal contaminant (Fig. 10a).

The higher Tb/Lu and Nb/La and Nb/Zr in the estimated primary alkali basalt relative to values for the sub-alkaline basalt suggest that strong positive Nb/La and Nb/Zr fractionation [$(Nb/Zr)_{AB}/(Nb/Zr)_{SAB} > 1{\cdot}4$] may have been caused by partial melting in the garnet stability field. This is not apparent in twin HFSE pairs, $(Zr/Hf)_{AB}/(Zr/Hf)_{SAB} \sim 1$ and $(Nb/Ta)_{AB}/(Nb/Ta)_{SAB} \sim 1$, yielding HFSE fractionation factors for Nb/Zr > Zr/Hf = Nb/Ta between primitive alkali and sub-alkaline basalts. Such Nb/Zr fractionation can be caused by major mantle mineral phases, including garnet, because D_{Nb} is almost always more than an order of magnitude smaller than D_{Zr} in these minerals (Green, 1994). Correlation of Nb/Zr and Tb/Lu also supports the role of garnet control for both element pairs (Fig. 10b). In the case of Nb/La, garnet would not fractionate these elements. However, cpx has D_{Nb} more than an order of magnitude lower than D_{La}, and could fractionate the element ratios (Green, 1995). Some mantle minerals, such as ilmenite or rutile, can fractionate Zr–Hf and Nb–Ta (Green, 1995). These minerals as mantle residues are commonly thought to cause HFSE depletion in arc sub-alkaline lavas (Ayers & Watson, 1993; Bodinier *et al.*, 1996), but this is not the case, or at least it is not prominent, in both the alkali and sub-alkaline basalt sources for the Ueno. Residual garnet and perhaps cpx phases during melting can account for the elevated HFSE abundances in the alkali basalt suite.

Consequently, concentrations of FME as well as LILE in the Ueno sub-alkaline basalt source need not be strongly elevated. The depletion in HFSE of the source is small and somewhat similar to that in MORB, and therefore the depletion observed in the evolved sub-alkaline basalt is not accounted for by mantle processes, but rather is a consequence of crustal assimilation. These observations suggest that arc signatures such as (1) isotopic EMII component enrichment, (2) relative FME enrichment, or (3) HFSE depletion found in the Ueno sub-alkaline basalts are largely due to assimilation of crustal materials. Even so, the isotopic, mineralogical, and geochemical characteristics of the alkali and sub-alkaline

source mantles should be distinct, and discrete domains are thus required.

Ueno mantle source processes: implications for arc basalt genesis

Mantle–crust process identification

Ujike & Stix (2000) proposed that the Ueno Basalts were unlikely to have originated from fluid-fluxed melting, but rather from decompression melting of a rising mantle diapir, which first generated alkali basalt and also melted mantle lithosphere to generate sub-alkaline basalt. This had already been proposed on the basis of geological and major element evidence (Kimura & Yoshida, 1999; Kimura *et al.*, 1999). The mantle sources for the alkali and sub-alkaline basalts are clearly distinct, and vertical mantle heterogeneity is perhaps correlated with the transition from the asthenosphere (alkali basalt source) to overlying enriched mantle lithosphere (sub-alkaline source) (Fig. 11c and d).

Apparent temporal and spatial variations in incompatible element ratios (e.g. increases in K/TiO_2, Rb/Nb, Ba/Zr, K/Nb) suggested by Nakano *et al.* (2000) and Ujike & Stix (2000) are unlikely to be controlled only by mantle processes, but may also be affected by intra-crustal AFC. This may reflect changes in the crustal stress regime associated with the province. Release of regional compressive stress in the crust may have occurred in the Ueno province in the early eruptive stage, allowing mantle-derived alkali and sub-alkaline basalts to ascend quickly, with less time to stagnate in the crust. This tensional stress field in the center of the province graded into compression toward the province perimeter (Kimura & Yoshida, 1999), giving a greater chance for magmatic stagnation and AFC to modify primitive basalts in the outer zone of the province, where lavas were erupted during the later stages of activity (see Figs 2 and 11). In fact, quartz-normative lavas, which provide the best evidence for extensive crustal assimilation, occur most frequently at the province margins.

In this framework, the chemically homogeneous primary sub-alkaline basalt type persisted over the life of the Ueno Basalts. The conclusion that a significant amount of crustal assimilation can be identified in fractionated sub-alkaline Ueno basalts contrasts with the conclusions of other researchers, who have tended to focus on the role of mantle heterogeneity.

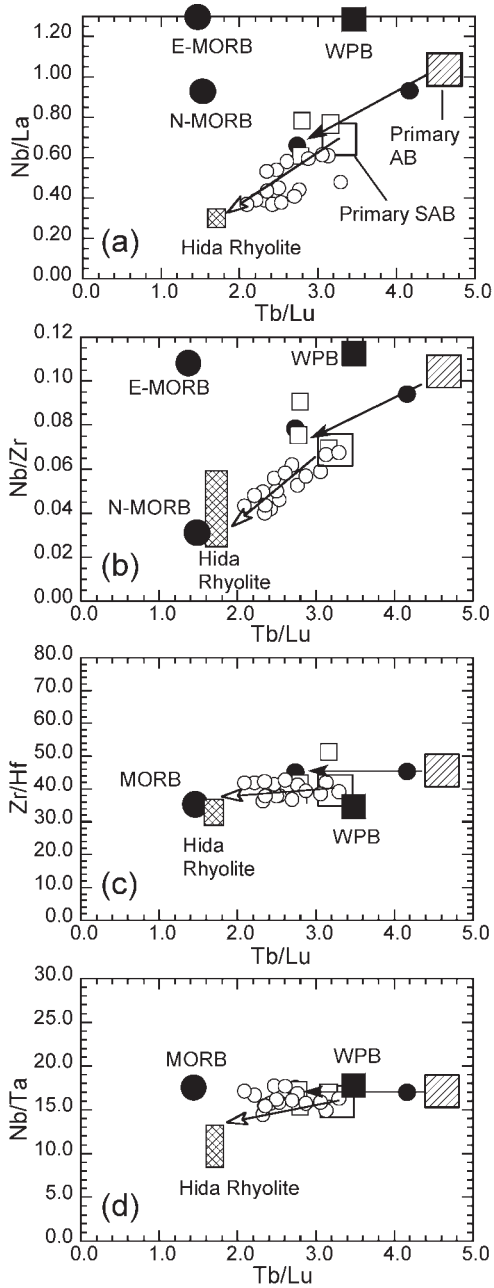

Fig. 10. HFSE ratios vs Tb/Lu ratio for Ueno Basalts lavas. The Tb/Lu (MREE/HREE) ratio reflects the role of residual garnet in melt generation. Nb/La (a), Nb/Zr (b) and Tb/Lu covary strongly. Boxes labeled 'Primary SAB' and 'Primary AB' mark the compositions of primitive sub-alkaline and alkali basalt, respectively. Linear arrays of sub-alkaline lavas reflect mixing between primary SAB and crust through AFC. Alkali–transitional basalt suite arrays indicate mixing between sub-alkaline and primary alkali basalt compositions. Crustal contaminant (e.g. Hida Rhyolite) compositions lie in the direction of the arrows with open arrowheads. HFSE ratios for the primary SAB and AB differ greatly in Nb/La and Nb/Zr, whereas these are very similar for Zr/Hf and Nb/Ta. This suggests similar behavior in the source between similar element pairs (Zr–Hf and Nb–Ta), and that Nb–Zr and Nb/La fractionation accompanies melting. WPB and MORB indicate incompatible element ratios for WPB, N-MORB and E-MORB (Sun & McDonough, 1989).

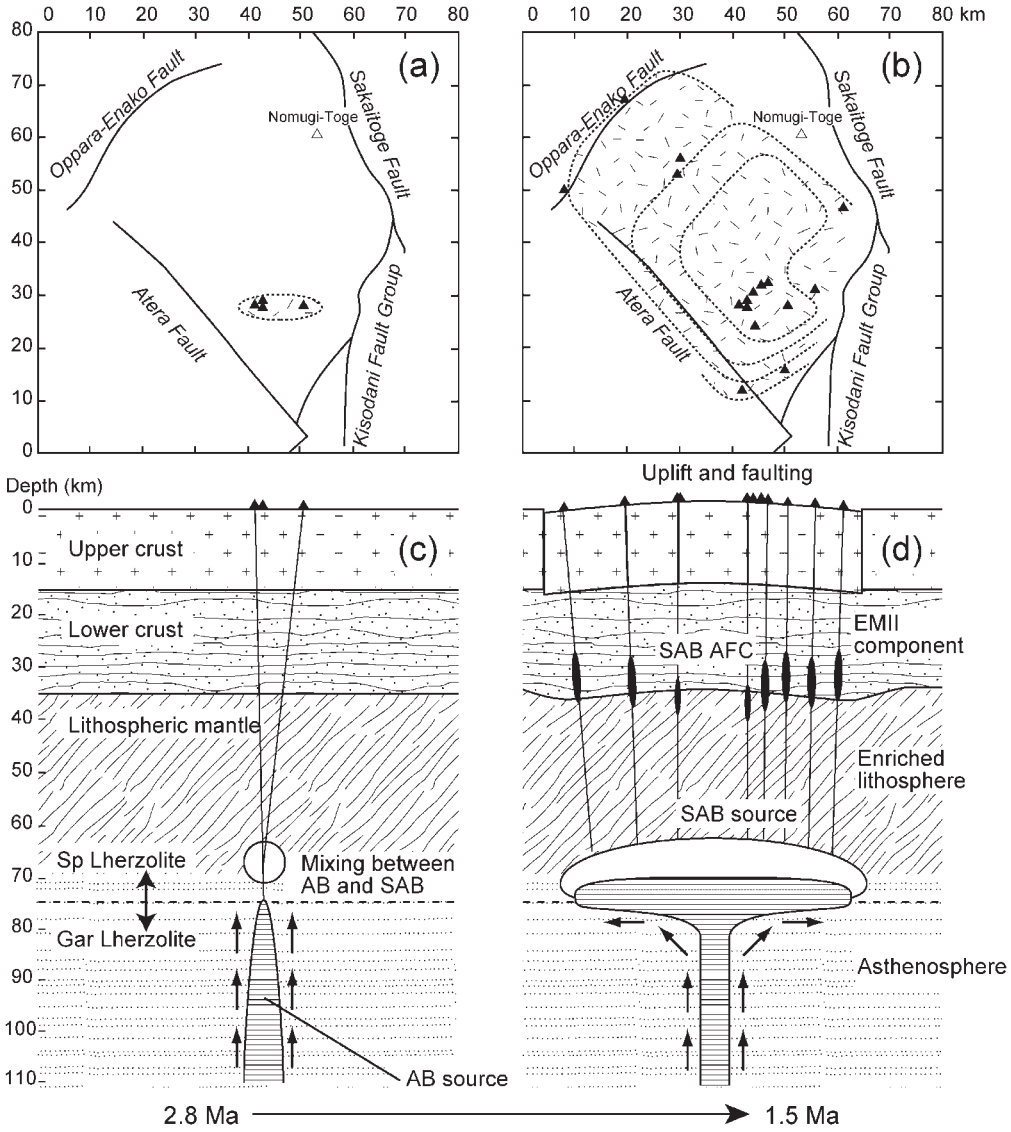

Fig. 11. Schematic representations of the temporal evolution of the Ueno Basalt Province (time increases to the right). The evolution is shown as cross-sections through the crust and mantle (c and d) and plan views of the surface (a and b). The rising mantle diapir induces melting of the overlying mantle lithosphere. Alkali basalts (AB) were produced from the deeper (athenospheric source) mantle diapir, whereas sub-alkaline basalts (SAB) were derived from isotopically enriched lithospheric mantle. Contemporaneous generation of AB and SAB during the first stage is suggested by evidence for chemical mixing between AB and SAB lavas. Lithosphere melting could have been caused by heat flux from the deep diapir. Segregated lavas would have stagnated near the Moho or within the lower crust, where AFC processes resulted in development of an EMII isotopic signature and increased fluid mobile element abundances in the SAB lavas. The HFSE-depleted nature of the SAB suite lavas also reflects crustal assimilation.

Mantle diapir or fluid-fluxed melting?

Either a mantle diapir mechanism or fluid-fluxed melting could maintain the Ueno sub-alkaline basalt reservoir for over 1·5 Myr. A continuous supply of heat or fluid is required to maintain basalt production for that order of time (McKenzie, 1984). The Ueno magmatic activity was intimately associated with regional uplift and migration of eruption centers, which are explained by flattening of the mantle diapir head (Kimura & Yoshida, 1999) or by buoyancy derived from partially molten bodies in the upper mantle produced by fluid-fluxed melting. Inferred mantle mineralogy and chemistry, observed isotopic compositions, and geobarometric results require spatially separate and chemically distinct mantle sources to produce the alkali basalt and sub-alkaline basalt magma types. The alkali basalt erupted first, both alone and contemporaneously with sub-alkaline basalt. Neither alkali basalts nor sub-alkaline basalts have strong signatures

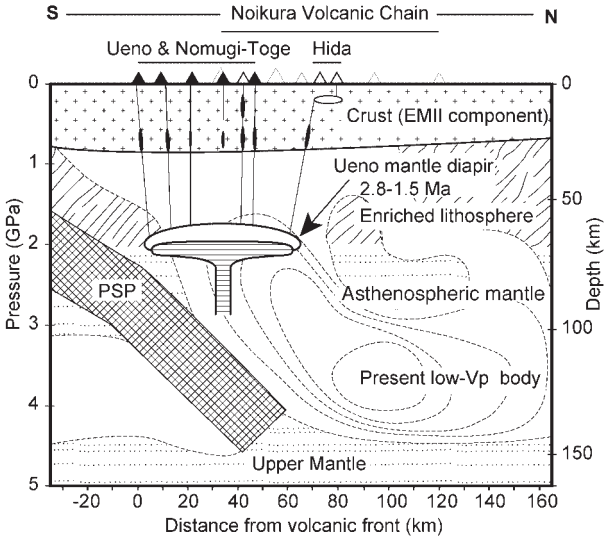

Fig. 12. Correlation between the Ueno mantle diapir and the P-wave velocity structure beneath the Norikura Volcanic Chain (Ando, 1986). Depths inferred for the Ueno mantle diapir agree with the depth of the low-V_p body. The source of the mantle diapir lies at a depth between 90 and 150 km, and the shallowest part of the diapir correlates with the upper part of the low-V_p body. The subducted Philippine Sea plate (PSP) may have lain well to the south during the Ueno activity. The Pacific plate is located at ~250 km depth beneath the area.

of fluid addition in their mantle source regions. We therefore prefer the mantle diapir model. The Ueno mantle diapir rose from the athenospheric mantle (>90 km) and melted first in the garnet-lherzolite stability field to produce alkali basalt (Fig. 11a and c). This rising diapir may have entrained and heated lithospheric mantle, which melted to yield sub-alkaline basalt, resulting in the observed association of alkali and sub-alkaline basalt. This process occurred in the spinel-lherzolite field (Fig. 11b and d). Continued ascent of the diapir head may also have uplifted the region, and flattening of the diapir head resulted in outward migration of eruption centers (Fig. 11b and d).

We consider that the incubating diapir model best explains the origin of the Ueno Basalts. The age range of the basalts matches the life span of such diapirs (Fig. 12). A similar model has also been proposed for the origin of alkali basalt clusters in SW Japan (Iwamori, 1991; Uto, 1996). Because the subducting Pacific plate lies at 250 km depth, any upwelling mantle must have originated shallower than this. What caused the mantle diapir to rise initially remains an unanswered question. Recent tomographic images of the mantle beneath the study area (Ando, 1986; Hasegawa *et al.*, 1991) show large volumes of low-V_p material. The main low-V_p body is located between 150 and 90 km depth, similar to the depth expected for the Ueno mantle diapir. The diapir today may have migrated to lie beneath the young (<1·3 Ma) Norikura Volcanic Chain (Ando, 1986; Kimura *et al.*, 1999). In its southern limit, the diapir lies close to 60 km deep, consistent with the pressure required for generating sub-alkaline basalt. The agreement of petrological inferences and seismic images provides further support for the mantle diapir model, and discussion of the origin of the deep mantle diapir (low-V_p body) is constrained by our understanding of the low-V_p upper mantle beneath this region. This, however, is beyond the scope of the present paper and will be discussed elsewhere.

Sources of island-arc basalt signatures

Relative depletion in HFSE and isotopic EMII enrichment are global characteristics of island-arc basalts (IAB). Ueno sub-alkaline basalts comprise a medium-K, calc-alkaline suite that possesses typical IAB characteristics. EMII isotopic components and fluid mobile elements were largely added as a result of crustal assimilation, as discussed above. We also consider that the relative depletion in Nb and Ta is largely due to crustal assimilation, although the depletion cannot be fully accounted for by this process alone. HFSE-depleted IAB-like signatures in the Ueno sub-alkaline basalts are thus inherited partly from enriched spinel-lherzolite facies mantle lithosphere. Depleted asthenospheric mantle, in turn, is considered to be the source of the Ueno alkali basalts, which also served as the heat source to produce sub-alkaline basalt through melting of the overlying enriched lithospheric mantle. The existence of enriched lithosphere and interaction between this and upwelling asthenosphere has been discussed previously in this area, but HFSE depletions have generally been attributed to fluids from the Pacific plate (Kaneko, 1995; Nakano *et al.*, 2000; Ujike & Stix, 2000). Our data argue against a large role for the addition of slab-derived fluid, and the coincidence of WPB-type alkali basalt with sub-alkaline basalt further supports the layered mantle–crust model.

Our interpretation for the origin of key IAB features differs from widely accepted models (Hawkesworth *et al.*, 1993; Davidson, 1996; Stolz *et al.*, 1996; Münker, 1998), which explain LILE and EMII enrichments by addition of fluid or sediment melts from the subducting slab to the overlying depleted mantle wedge. However, we believe that our scheme best explains the geology, petrology, geochemistry, and the history of the Ueno Basalt lavas, and therefore should be tested in other basalt suites associated with continental arcs.

CONCLUSION

We have studied the major and trace element, and Sr, Nd and Pb isotope geochemistry of the Ueno Basalts in central Japan. The Ueno Basalts are geologically well known and are considered to be derived from a common

mantle diapir. WPB-type alkali basalt and IAB-type sub-alkaline basalt occur in the Ueno suite and are derived from melting of depleted MORB-source (garnet-lherzolite facies) and shallow enriched (spinel-lherzolite facies) sources, respectively. Apparent low abundances of Nb and Ta in the sub-alkaline basalts are due partly to residual minerals in the source that host HFSE, such as ilmenite, but mostly to relative enrichment of LILE and depletion in HFSE by crustal assimilation. EMII isotopic components and fluid mobile element enrichments found in IAB-type basalts are mainly due to contamination of melts by local crust, and at least two crustal contaminants can be identified. The role of crustal contamination is significant and enrichment of the mantle source by slab-derived fluids is not responsible for the IAB characteristics of the Ueno sub-alkaline basalts. The chemical diversity observed in the Ueno Basalts originates from two mantle and two crustal components, which appear to be grossly stratified beneath the area. Contemporaneous eruption of the WPB and IAB suites suggests an incubating depleted mantle diapir, which rose, flattened, and melted overlying enriched lithospheric mantle. This petrological model is consistent with regional uplift and the outward migration of the eruption centers. The mantle diapir model proposed here explains the coincidence of WPB- and IAB-type basalts in island-arc settings, and may be a mechanism for generating island-arc-type basalt in continental margin arcs.

ACKNOWLEDGEMENTS

Our thanks go to Professors Y. Nagahashi, S. Harayama and Y. Komuro, and Dr. Barry Roser for discussions, and to Professor K. Manabe, who kindly permitted free access to X-ray fluorescence spectrometry facilities at Fukushima University. Reviews by Professors R. Arculus and J. Gamble have improved this paper. This research was supported by grants-in-aid of the Ministry of Education, Science, and Culture, Japan, 10304038 and 12874058 (Rep. J.-I. Kimura), 11640451 (Rep. S. Iizumi), 1440150 (Rep. A. Takasu), 11640454 (Rep. S. Sano), and 12304031 (Rep. T. Yoshida).

REFERENCES

Ando, M. (1986). Mantle diapirs observed in the seismic window. *Bulletin of the Volcanological Society of Japan* **31**, 45–53.

Arakawa, Y. (1990). Two types of granitic intrusions in the Hida belt, Japan: Sr isotopic and chemical characteristics of the Mesozoic Funatsu granitic rocks. *Chemical Geology* **85**, 101–117.

Aramaki, S. & Ui, T. (1982). Japan. In: Thorpe, R. S. (ed.) *Andesites: Orogenic Andesites and Related Rocks*. Chichester: Wiley, pp. 259–292.

Ayers, J. C. & Watson, E. B. (1993). Rutile solubility and mobility in supercritical aqueous fluids. *Contributions to Mineralogy and Petrology* **114**, 321–330.

Bebout, G. E., Ryan, J. G., Leeman, W. P. & Bebout, A. E. (1999). Fractionation of trace elements by subduction-zone metamorphism—effect of convergent-margin thermal evolution. *Earth and Planetary Science Letters* **171**, 63–81.

Bodinier, J.-L., Merlet, C., Bedini, R. M., Simien, F., Remaidi, M. & Garrido, C. J. (1996). Distribution of niobium, tantalum, and other highly incompatible trace elements in the lithospheric mantle: the spinel paradox. *Geochimica et Cosmochimica Acta* **60**, 545–550.

Caroff, M., Maury, R. C., Guille, G. & Cotten, J. (1997). Partial melting below Tubuai (Austral Islands, French Polynesia). *Contributions to Mineralogy and Petrology* **127**, 369–382.

Davidson, J. P. (1996). Deciphering mantle and crustal signatures in subduction zone magmatism. *Subduction Top to Bottom, Geophysical Monograph, American Geophysical Union* **96**, 251–262.

Feigenson, M. D., Hofmann, A. W. & Spera, F. J. (1983). Case studies on the origin of basalt. II. The transition from tholeiitic to alkalic volcanism on Kohara volcano, Hawaii. *Contributions to Mineralogy and Petrology* **84**, 390–405.

Flower, M. F. J., Russo, R. M., Tamaki, K. & Hoang, N. (2001). Mantle contamination and the Izu–Bonin–Mariana (IBM) 'high-tide-mark': evidence for mantle extrusion caused by Tethyan closure. *Tectonophysics* **333**, 9–34.

Ghiorso, M. S. & Sack, R. O. (1995). Chemical mass transfer in magmatic processes IV. A revised and internally consistent thermodynamic model for the interpolation and extrapolation of liquid–solid equilibria in magmatic systems at elevated temperatures and pressures. *Contributions to Mineralogy and Petrology* **119**, 197–212.

Gill, J. B. (1981). *Orogenic Andesites and Plate Tectonics*. Heidelberg: Springer.

Green, D. H. & Ringwood, A. E. (1967). The stability fields of aluminous pyroxene peridotite and garnet peridotite and their relevance in upper mantle structure. *Earth and Planetary Science Letters* **3**, 151–160.

Green, T. H. (1994). Experimental studies of trace-element partitioning applicable to igneous petrogenesis—Sedona 16 years later. *Chemical Geology* **117**, 1–36.

Green, T. H. (1995). Significance of Nb/Ta as an indicator of geochemical processes in the crust–mantle system. *Chemical Geology* **120**, 347–359.

Halliday, A. N., Lee, D.-C., Tommasini, S., Davies, G. R., Paslick, C. R., Fitton, J. G. & James, D. E. (1995). Incompatible trace elements in OIB and MORB and source enrichment in sub-oceanic mantle. *Earth and Planetary Science Letters* **133**, 379–395.

Harayama, S. (1990). *Geology of the Kamikochi District with Geological Sheet Map at 1:50 000*. Tsukuba: Geological Survey of Japan.

Harayama, S., Takeuchi, M., Nakano, S., Sato, T. & Takizawa, F. (1991). *Geology of the Yarigatake District with Geological Sheet Map at 1: 50 000*. Tsukuba: Geological Survey of Japan.

Hart, S. R. (1984). The DUPAL anomaly: a large scale isotopic anomaly in the southern hemisphere. *Nature* **309**, 753–756.

Hasegawa, A., Zhao, D., Hori, S., Yamamoto, A. & Horiuchi, S. (1991). Deep structure of the northeastern Japan arc and its relationship to seismic and volcanic activity. *Nature* **352**, 683–689.

Hawkesworth, C. J., Gallagher, K., Hergt, J. M. & McDermott, F. (1993). Trace element fractionation processes in the generation of island arc basalts. *Philosphical Transactions of the Royal Society of London, Series A* **342**, 179–191.

Hickey-Vargas, R., Hergt, J. M. & Spadea, P. (1995). The Indian Ocean-type isotopic signature in Western Pacific marginal basins: origin and significance. In: Taylor B. & Natland J. (eds) *Active Margins and Marginal Basins of the Western Pacific. Geophysical Monograph, American Geophysical Union* **88**, 175–197.

Hiroi, Y. (1981). Subdivision of the Hida metamorphic complex, Central Japan, and its bearing on the geology of the Far East in pre-Sea of Japan time. *Tectonophysics* **76**, 317–333.

Iizumi, S., Maehara, K., Morris, P. A. & Sawada, Y. (1994). Sr isotope data of some GSJ rock reference samples. *Memoir of Faculty of Science, Shimane University* **28**, 83–86.

Iizumi, S., Morris, P. A. & Sawada, Y. (1995). Nd isotope data for GSJ reference samples JB-1a, JB-3 and JG-1a and the La Jolla standard. *Memoir of Faculty of Science, Shimane University* **29**, 73–76.

Iwamori, H. (1991). Zonal structure of Cenozoic basalts related to mantle upwelling in southwest Japan. *Journal of Geophysical Research* **96**, 6157–6170.

Johannes, H. & Holtz, F. (1996). *Petrogenesis and Experimental Petrology of Granitic Rocks*. Heidelberg: Springer.

Kaneko, T. (1995). Geochemistry of Quaternary basaltic lavas in the Norikura area, central Japan: influence of the subcontinental upper mantle on the trace elements and Sr isotope compositions. *Journal of Volcanology and Geothermal Research* **64**, 61–83.

Kelemen, P. B., Hart, S. R. & Bernstein, S. (1998). Silica enrichment in the continental upper mantle via melt/rock reaction. *Earth and Planetary Science Letters* **164**, 387–406.

Kersting, A. B., Arculus, R. J. & Gust, D. A. (1996). Lithospheric contributions to arc magmatism: isotope variations along strike in volcanoes of Honshu, Japan. *Science* **272**, 1464–1468.

Kimura, J.-I. & Yamada, Y. (1996). Evaluation of major and trace element XRF analyses using a flux to sample ratio of two to one glass beads. *Journal of Mineralogy, Petrology, and Economic Geology* **91**, 62–72.

Kimura, J.-I. & Yoshida, T. (1999). Mantle diapir induced arc volcanism: the Ueno Basalts, Nomugi-Toge and Hida volcanic suites, central Japan. *Island Arc* **8**, 304–322.

Kimura, J.-I., Yoshida, T. & Nagahashi, Y. (1999). Magma plumbing systems and seismic structures: inferences from the Norikura Volcanic Chain, central Japan. *Memoir of the Geological Society of Japan* **53**, 157–175.

Kimura, J.-I., Yoshida, T. & Takaku, Y. (1995). Igneous rock analysis using ICP-MS with internal standardization, isobaric ion overlap correction, and standard addition methods. *Science Report of Fukushima University* **56**, 1–12.

Klein, E. M. & Langmuir, C. H. (1987). Global correlations of oceanic ridge basalt chemistry with axial depth and crustal thickness. *Journal of Geophysical Research* **92**, 8089–8115.

Kushiro, I. (1994). Recent experimental studies on partial melting of mantle peridotites at high pressures using diamond aggregates. *Journal of Geological Society of Japan* **100**, 103–110.

Le Maitre, R. W., Bateman, P., Dudek, A., Keller, J., Lameyre, J., Le Bas, M. J., Sabine, P. A., Schmid, R., Sorensen, H., Streckeisen, A., Woolley, A. R. & Zanettin, B. (1989). *A Classification of Igneous Rocks and Glossary of Terms*. Oxford: Blackwell.

Manton, W. I. (1988). Separation of Pb from young zircons by single-bead ion exchange. *Chemical Geology* **73**, 147–152.

Matsuda, T. (1978). Collision of the Izu–Bonin arc with central Honshu, Cenozoic tectonics of the Fossa Magna, Japan. *Journal of the Physics of the Earth* **26**, 409–421.

Matsumoto, A. & Kobayashi, T. (1999). K–Ar ages of the older On-take volcanic products, On-take Volcano, central Japan: reappraisal of the volcanic history based on radiometric data. *Journal of the Volcanological Society of Japan* **44**, 1–12.

McKenzie, D. (1984). The generation and compaction of partially molten rock. *Journal of Petrology* **25**, 713–765.

Miyashiro, A. (1978). Nature of alkaline volcanic series. *Contributions to Mineralogy and Petrology* **66**, 91–104.

Münker, C. (1998). Nb/Ta fractionation in a Cambrian arc/back arc system, New Zealand: source constraints and application of refined ICPMS techniques. *Chemical Geology* **144**, 23–45.

Nakano, S. (1993). Ueno basaltic rocks I: Heterogeneous magmas at two monogenetic volcanoes. *Journal of Mineralogy, Petrology, and Economic Geology* **88**, 272–288.

Nakano, S. (1994). Ueno basaltic rocks II: Chemical variation in the Kiso province south of the Ontake volcano. *Journal of Mineralogy, Petrology, and Economic Geology* **89**, 115–130.

Nakano, S., Uto, K. & Uchiumi, S. (2000). K–Ar ages and temporal chemical variation of the Ueno Basaltic Rocks and Jizo-toge Volcanic Rocks, central Japan. *Journal of Volcanological Society of Japan* **45**, 87–105.

Notsu, K., Arakawa, Y., Nakano, S. & Yamasaki, M. (1989). Lateral variations in $^{87}Sr/^{86}Sr$ ratios of volcanic rocks from central Japan. *Geochemical Journal* **23**, 45–55.

Okamura, S., Arculus, R. J., Marthynov, Y. A., Kagami, H., Yoshida, T. & Kawano, Y. (1998). Multiple magma sources involved in marginal-sea formation: Pb, Sr, and Nd isotopic evidences from the Japan Sea region. *Geology* **26**, 619–622.

Otofuji, Y., Hayashida, A. & Torii, M. (1985). When was the Japan Sea opened?: Paleomagnetic evidence from southwest Japan. In: Nasu, N. (ed.) *Formation of Active Ocean Margins*. Tokyo: Terrapub, pp. 551–566.

Otofuji, Y., Kambara, A., Matsuda, T. & Nohda, S. (1994). Counterclockwise rotation of Northeast Japan: paleomagnetic evidence for regional extent and timing of rotation. *Earth and Planetary Science Letters* **121**, 503–518.

Otsuka, T. (1988). Paleozoic–Mesozoic sedimentary complex in the eastern Mino Terrane, central Japan. *Journal of Geoscience of Osaka City University* **31**, 63–122.

Pouclet, A., Lee, J.-S., Vidal, P., Cousens, B. & Bellon, H. (1995). Cretaceous to Cenozoic volcanism in South Korea and in the Sea of Japan: magmatic constraints on the opening of the back-arc basin. In: Smellie, J. L. (ed.) *Volcanism Associated with Extension at Consuming Plate Margins. Geological Society, London, Special Publications* **81**, 169–191.

Putirka, K., Johnson, M., Kinzler, R., Longi, J. & Walker, D. (1995). Thermobarometry of mafic igneous rocks based on clinopyroxene–liquid equilibria, 0–30 kbar. *Contributions to Mineralogy and Petrology* **123**, 92–108.

Robinson, J. A. & Wood, B. J. (1998). The depth of the spinel to garnet transition at the peridotite solidus. *Earth and Planetary Science Letters* **164**, 277–284.

Rollinson, H. (1993). *Using Geochemical Data: Evaluation, Presentation, Interpretation*. Harlow, UK: Longman.

Saunders, A. D. & Tarney, J. (1984). Geochemical characteristics of basaltic volcanism within back-arc basins. In: Kokelaar, B. P. & Howells, M. F. (eds) *Marginal Basin Geology. Geological Society, London, Special Publications* **16**, 59–76.

Shaw, D. M. (1970). Trace element fractionation during anatexis. *Geochimica et Cosmochimica Acta* **34**, 237–243.

Shibata, T. & Nakamura, E. (1997). Across-arc variations of isotope and trace element compositions from Quaternary basaltic volcanic rocks in northeastern Japan: implications for interaction between subducted oceanic slab and mantle wedge. *Journal of Geophysical Research B* **102**, 8051–8064.

Shimizu, S. & Itaya, T. (1993). Plio-Pleistocene arc magmatism controlled by overlapping subducted plates, central Japan. *Tectonophysics* **225**, 139–154.

Shimoda, G., Tatsumi, Y., Nohda, S., Ishizaka, K. & Jahn, B. M. (1998). Setouchi high-Mg andesites revisited: geochemical evidence for melting of subducting sediments. *Earth and Planetary Science Letters* **160**, 479–492.

Stolz, A. J., Jochum, K. P., Spettel, B. & Hofmann, A. W. (1996). Fluid- and melt-related enrichment in the subarc mantle: evidence from Nb/Ta variations in island-arc basalts. *Geology* **24**, 587–590.

Sun, S.-s. & McDonough, W. F. (1989). Chemical and isotopic systematics of oceanic basalts: implications for mantle composition and processes. In Saunders, A. D. & Norry, M. J. (eds) *Magmatism in the Ocean Basins. Geological Society, London, Special Publications* **42**, 313–345.

Takahashi, E. & Kushiro, I. (1983). Melting of a dry peridotite at high pressures and basalt magma genesis. *American Mineralogist* **68**, 859–879.

Takeuchi, A. (1995). Changes in regional stress field and volcanic activity: formation history of the Chubu Mountain Range. *Chikyu Monthly* **200**, 92–96.

Tanaka, S. (1992). Origin of the Early Mesozoic granitic rocks in the Hida Terrane, Japan, and its implication for evolution of the continental crust. *Journal of Sciences, Hiroshima University* **9**(3), 435–493.

Taylor, S. R. & McLennan, S. M. (1985). *The Continental Crust: its Composition and Evolution*. Oxford: Blackwell.

Thompson, R. N. (1982). British Tertiary volcanic province. *Scottish Journal of Geology* **18**, 49–107.

Turner, S., Hawkesworth, C. J., Rogers, N., Bartlett, J., Worthington, T., Hergt, J., Pearce, J. & Smith, I. E. M. (1997). ^{238}U–^{230}Th disequilibria, magma petrogenesis, and flux rates beneath the depleted Tonga–Kermadec island arc. *Geochimica et Cosmochimica Acta* **61**, 4855–4884.

Turner, S., McDermott, F., Hawkesworth, C. & Kepezhinskas, P. (1998). A U-series study of lavas from Kamchatka and the Aleutians: constraints on source composition and melting processes. *Contributions to Mineralogy and Petrology* **133**, 217–234.

Ujike, O., Iizuka, Y. & Nakano, S. (1992). K–Ar ages of the Ueno basaltic rocks. *Journal of Mineralogy, Petrology, and Economic Geology* **87**, 102–106.

Ujike, O. & Stix, J. (2000). Geochemistry and origins of Ueno and On-take basaltic to andesitic rocks (<3 Ma) produced by distinct contributions of subduction components, central Japan. *Journal of Volcanology and Geothermal Research* **95**, 49–64.

Uto, K. (1996). Volcanoes and age determination: now and future of K–Ar and 40Ar/39Ar dating. *Bulletin of the Volcanological Society of Japan* **40**, S27–S46.

Weaver, B. & Tarney, J. (1984). Empirical approach to estimating the continental crust. *Nature* **310**, 575–577.

Wood, D. A., Joron, J. L., Treuil, M., Norry, M. & Tarney, J. (1979). Element and Sr isotope variations in basic lavas from Iceland and the surrounding ocean floor. *Contributions to Mineralogy and Petrology* **70**, 319–339.

Yamada, N. (1977). Nohi Rhyolite and associated granitic rocks. In: Yamada, N. (ed.) *Mesozoic Felsic Igneous Activity and Related Metamorphism in Central Japan—From Nagoya to Toyama. Guidebook for Excursion 4*. Tsukuba: Geological Survey of Japan.

Yamada, N. & Kobayashi, T. (1988). *Geology of the Ontake District with Geological Sheet Map at 1:50 000*. Tsukuba: Geological Survey of Japan.

Zhao, D., Horiuchi, S. & Hasegawa, A. (1992). Seismic velocity structure of the crust beneath the Japanese Islands. *Tectonophysics* **212**, 289–301.

Zindler, A. & Hart, S. (1986). Chemical geodynamics. *Annual Review of Earth and Planetary Sciences* **14**, 493–571.